

1      The effects of multi-dimensional drought on land cover change and  
2      vegetation productivity in continental Chile

3      Francisco Zambrano<sup>a,b,1,\*</sup>, Anton Vrieling<sup>c</sup>, Francisco Meza, Iongel Duran-Llacer, Francisco Fernández<sup>d</sup>,  
4      Alejandro Venegas-González, Nicolas Raab, Dylan Craven

<sup>a</sup> Universidad Mayor, Hémera Centro de Observación de la Tierra, Facultad de Ciencias, Escuela de Ingeniería en Medio Ambiente y Sustentabilidad, Santiago, Chile, 7500994

<sup>b</sup> Universidad Mayor, Observatorio de Sequía para la Agricultura y la Biodiversidad de Chile (ODES),

<sup>c</sup> University of Twente, Faculty of Geo-Information Science and Earth Observation (ITC), Enschede, The Netherlands,

<sup>d</sup> Universidad San Sebastian,

---

5      **Abstract**

The north-central region of Chile has been the focus of research studies due to the persistent decrease in water supply, which is impacting the hydrological system and vegetation development. This persistent period of water scarcity has been defined as a mega-drought. The aim of our study is to evaluate the interaction of drought, land cover change, and vegetation productivity over continental Chile. We used drought indices for atmospheric evaporative demand (AED), water supply, and soil moisture from short-term (1, 3, 6 months) to long-term (12, 24, 36 months) time scales. We derived the drought indices using monthly ERA5-Land reanalysis data spanning from 1981 to 2023. We utilized the Moderate-Resolution Imaging Spectroradiometer (MODIS) datasets to derive information on annual land cover and monthly vegetation productivity. Our results showed that from south to north, Chile has a declining trend in water supply, and across the whole country, there is an increase in AED. These trends are stronger at longer time scales. The trend in vegetation productivity in the north-central area is affecting, to a higher degree, shrubland and savanna, followed by croplands and forests. The drought explains about 30% of the change in land cover type across Chile for forest, grassland, shrubland, and savanna. The increase in AED is the main driver of the change in land cover, followed by a reduction in precipitation and soil moisture. The change in vegetation productivity has been severe in the north-central part of the country for all land cover types, particularly savanna, shrubland, and croplands. The anomaly in soil moisture over the past 12 months (SSI-12) is the main variable explaining these changes, followed by anomalies in cumulated precipitation over one to two years (SPI-12 and SPI-24). Our results provide insightful information that would help in developing adaptation measures for ecosystems in Chile to cope with climate change and drought.

6      **Keywords:** drought, land cover change, vegetation productivity, satellite

---

7      **1. Introduction**

8      Drought is often classified as meteorological when there is a decrease in precipitation below the mean  
9      average of several years (more than 30 years), hydrological when these anomalies last for long periods (months

---

\*Corresponding author

Email addresses: francisco.zambrano@umayor.cl (Francisco Zambrano), a.vrieling@utwente.nl (Anton Vrieling), francisco.fernandez@uss.cl (Francisco Fernández)

<sup>1</sup>This is the first author footnote.

to years) and affect water systems, and agricultural when the deficit impacts plant health anomalies and leads to decreased productivity (Wilhite and Glantz, 1985). However, it is important to note that drought is also influenced by human activities, which were not considered in the definitions. Thus, Van Loon et al. (2016) and AghaKouchak et al. (2021) have given an updated definition of drought for the Anthropocene, suggesting that it should be considered the feedback of humans' decisions and activities that drives the anthropogenic drought. Simultaneously, drought leads to heightened tree mortality and induces alterations in land cover and land use, ultimately affecting ecosystems (Crausbay et al., 2017). Even though many ecological studies have misinterpreted how to characterize drought, for example, sometimes considering "dry" conditions as "drought" (Slette et al., 2019). Then, Crausbay et al. (2017) proposed the ecological drought definition as "an episodic deficit in water availability that drives ecosystems beyond thresholds of vulnerability, impacts ecosystem services, and triggers feedback in natural and/or human systems." In light of current global warming, it is crucial to study the interaction between drought and ecosystems in order to understand their feedback and impact on water security. (Bakker, 2012)

Human-induced greenhouse gas emissions have increased the frequency and/or intensity of drought as a result of global warming, according to the sixth assessment report (AR6) of the Intergovernmental Panel on Climate Change (IPCC) (Calvin et al., 2023). The evidence supporting this claim has been strengthened since AR5 (IPCC, 2013). Recent studies, however, have produced contrasting findings, suggesting that drought has not exhibited a significant trend over the past forty years. (Vicente-Serrano et al., 2022; Kogan et al., 2020). Vicente-Serrano et al. (2022) analyzed the meteorological drought trend on a global scale, finding that only in a few regions has there been an increase in the severity of drought. Moreover, they attribute the increase in droughts over the past forty years solely to an increase in atmospheric evaporative demand (AED), which in turn enhances vegetation water demand, with important implications for agricultural and ecological droughts. Also, they state that "the increase in hydrological droughts has been primarily observed in regions with high water demand and land cover change". Similarly, Kogan et al. (2020) analyzed the drought trend using vegetation health methods, finding that for the globe, hemispheres, and main grain-producing countries, drought has not expanded or intensified for the last 38 years. Further, Masson-Delmotte (2021) suggests that there is a high degree of confidence that rising temperatures will increase the extent, frequency, and severity of droughts. Also, AR6 (Calvin et al., 2023) predicts that many regions of the world will experience more severe agricultural and ecological droughts even if global warming stabilizes at 1.5°–2°C. To better evaluate the impact of drought trends on ecosystems, assessments are needed that relate meteorological and soil moisture variables to their effects on vegetation.

From 1960 to 2019, land use change has impacted around one-third of the Earth's surface, which is four times more than previously thought (Winkler et al., 2021). Multiple studies aim to analyze and forecast changes in land cover globally (Winkler et al., 2021; Song et al., 2018) and regionally (Chamling and Bera, 2020; Homer et al., 2020; Yang and Huang, 2021). Some others seek to analyze the impact of land cover change on climate conditions such as temperature and precipitation (Luyssaert et al., 2014; Pitman et al., 2012). There is less research on the interaction between drought and land cover change (Chen et al., 2022; Akinyemi, 2021; Peng et al., 2017). Peng et al. (2017) conducted a worldwide investigation utilizing net primary production to examine the spatial and temporal variations in vegetation productivity at global level. The study aimed to assess the influence of drought by comparing the twelve-month Standardized Precipitation Evapotranspiration Index (SPEI) and land cover change. According to their findings, drought is responsible for 37% of the decline in vegetation productivity, while water availability accounts for 55% of the variation. Chen et al. (2022) studied the trend of vegetation greenness and productivity and its relation to meteorological drought (SPEI of twelve months in December) and soil moisture at the global level. The results showed lower correlations (<0.2) for both variables. Akinyemi (2021) evaluates drought trends and land cover change using vegetation indices in Botswana in a semi-arid climate. These studies mostly looked at how changes in land cover and vegetation productivity are related to a single drought index (SPEI) over a single time period of 12 months. SPEI takes into account the combined effect of precipitation and AED as a water balance, but it does not allow us to know the contribution of each variable on its own. Some things worth investigating in terms of land cover change and vegetation productivity are: i) How do they respond to short- to long-term meteorological and soil moisture droughts? ii) How is the drought impacting land

61 cover changes? And iii) How do they behave in humid and arid climatic zones regarding drought? Likewise,  
62 there is a lack of understanding of how the alteration in water supply and demand is affecting land cover  
63 transformations.

64 For monitoring drought, the World Meteorological Organization recommends the SPI (Standardized Pre-  
65 cipitation Index) ([WMO et al., 2012](#)). The SPI is a multi-scalar drought index that only uses precipitation  
66 to assess short- to long-term droughts. The primary cause of drought is precipitation anomalies, and tem-  
67 perature usually makes it worse ([Luo et al., 2017](#)). Nowadays, there is an increase in attention toward  
68 using AED separately to monitor droughts ([Vicente-Serrano et al., 2020](#)). One reason is due to its attri-  
69 bution to increasing flash droughts in water-limited regions ([Noguera et al., 2022](#)). [Vicente-Serrano et al.](#)  
70 ([2010](#)) proposed the Standardized Precipitation Evapotranspiration Index (SPEI), which incorporated the  
71 temperature effect by subtracting AED from precipitation. SPEI allows for analysis of the combined effect  
72 of precipitation and AED. Since its formulation, it has been used worldwide for the study and monitoring  
73 of drought ([Gebrechorkos et al., 2023; Liu et al., 2024](#)). [Hobbins et al. \(2016\)](#) and [McEvoy et al. \(2016\)](#)  
74 developed the Evaporative Demand Drought Index (EDDI) to monitor droughts solely using the AED, and  
75 it has proven effective in monitoring flash droughts ([Li et al., 2024; Ford et al., 2023](#)). For soil moisture,  
76 several drought indices exist, such as the Soil Moisture Deficit Index (SDMI) ([Narasimhan and Srinivasan,](#)  
77 [2005](#)) and the Soil Moisture Agricultural Drought Index (SMADI) ([Souza et al., 2021](#)). [Hao and AghaK-](#)  
78 [ouchak \(2013\)](#) and [AghaKouchak \(2014\)](#) proposed the Standardized Soil Moisture Index (SSI), which has a  
79 similar formulation as the SPI, SPEI, and EDDI. Thus, there are plenty of drought indices that allow for  
80 a comprehensive assessment of drought on short- to long-term scales and that allow for the use of single  
81 variables from the earth's water balance (e.g., precipitation, AED, soil moisture). The variation in climate  
82 variables impacts vegetation development, and unfavorable conditions such as low precipitation and high  
83 temperatures usually generate a decrease in vegetation productivity. To monitor the response of vegetation,  
84 the common practice is to use satellite data. The Normalized Difference Vegetation Index (NDVI) has been  
85 widely used as a proxy for biomass production ([Camps-Valls et al., 2021; Paruelo et al., 2016; Helman et al.,](#)  
86 [2014](#)). For Chile's cultivated land, [Zambrano et al. \(2018\)](#) introduced the zcNDVI for assessing seasonal  
87 biomass production in response to drought. Using this information, we can advance our understanding of  
88 the impact of drought on ecosystems.

89 Chile's diverse climatic and ecosystem types ([Beck et al., 2023; Luebert and Pliscoff, 2022](#)) make it an ideal  
90 natural laboratory for studying climate and ecosystems. Additionally, the country has experienced severe  
91 drought conditions that have had significant effects on vegetation and water storage. North-central Chile has  
92 faced a persistent precipitation deficit since 2010, defined as a mega drought. ([Garreaud et al., 2017](#)), which  
93 has impacted the Chilean ecosystem. This megadrought was defined by the Standardized Precipitation  
94 Index (SPI) of twelve months in December having values below one standard deviation. Some studies have  
95 addressed how this drought affects single ecosystems in terms of forest development ([Miranda et al., 2020;](#)  
96 [Venegas-González et al., 2018](#)), forest fire occurrence ([Urrutia-Jalabert et al., 2018](#)), and crop productivity  
97 ([Zambrano, 2023; Zambrano et al., 2018, 2016](#)). We found one study regarding land cover and drought in  
98 Chile. The study by [Fuentes et al. \(2021\)](#) evaluates water scarcity and land cover change in Chile between  
99 29° and 39° of south latitude. [Fuentes et al. \(2021\)](#) used the SPEI of one month for evaluating drought,  
100 which led to misleading results. For example, they did not find a temporal trend in the SPEI but found a  
101 decreasing trend in water availability and an increase trend on AED, which in turn should have been capable  
102 of being captured with longer time scales of the SPEI. The term "megadrought" in Chile is used to describe  
103 a prolonged water shortage that lasts for several years, resulting in a permanent deficit that impacts the  
104 hydrological system ([Boisier et al., 2018](#)). Therefore, it is crucial to evaluate temporal scales that consider  
105 the cumulative impact over a period of several years. The association between drought and the environment  
106 in Chile is not well comprehended. Hence, it is imperative to acquire a more profound comprehension of the  
107 manner in which climatic and soil moisture droughts influence environmental dynamics, in order to make  
108 well-informed decisions on adaptation strategies.

109 Here, we analyze the multi-dimensional impacts of drought across ecosystems in continental Chile. More  
110 specifically, we aim to assess: i) short- to long-term temporal trends in multi-scalar drought indices; ii)

111 temporal changes in land-use cover and the direction and magnitude of their relationships with trends in  
 112 drought indices; and iii) the trend in vegetation productivity and its relationship with drought indices across  
 113 Chilean ecosystems.

## 114 2. Study area

115 Continental Chile has diverse climate conditions with strong gradients from north to south and east to west  
 116 (Aceituno et al., 2021) (Figure 1 a), which determines its great ecosystem diversity (Luebert and Pliscoff,  
 117 2022) (Figure 1 c). The Andes Mountains are a main factor in climate latitudinal variation (Garreaud, 2009).  
 118 “Norte Grande” and “Norte Chico” predominate in an arid desert climate with hot (Bwh) and cold (Bwk)  
 119 temperatures. At the south of “Norte Chico,” the climate changes to an arid steppe with cold temperatures  
 120 (Bsk). In these two northern regions, the land is mostly bare, with a small surface of vegetation types  
 121 such as shrubland and grassland. In the zones “Centro” and the north half of “Sur,” the main climate is  
 122 Mediterranean, with warm to hot summers (Csa and Csb). Land cover in “Centro” comprises a significant  
 123 amount of shrubland and savanna (50%), grassland (16%), forest (8%), and croplands (5%). An oceanic  
 124 climate (Cfb) predominates in the south of “Sur” and the north of “Austral.” Those zones are high in forest  
 125 and grassland. The southern part of the country has a tundra climate, and in “Austral,” it is a cold semi-arid  
 126 area with an extended surface of grassland, forest, and, to a lesser extent, savanna.

## 127 3. Materials and Methods

### 128 3.1. Data

#### 129 3.1.1. Gridded meteorological and vegetation data

130 To analyze land cover change, we use the classification scheme by the IGBP (International Geosphere-  
 131 Biosphere Programme) from the product MCD12Q1 collection 6.1 from MODIS. The MCD12Q1 has a  
 132 yearly frequency from 2001 to 2022 and defines 17 classes. To derive a proxy for vegetation productivity, we  
 133 used the Normalized Difference Vegetation Index (NDVI) from the product MOD13A3 collection 6.1 from  
 134 MODIS (Didan, 2015). MOD13A3 provides vegetation indices at 1km of spatial resolution and monthly  
 135 frequency. The NASA EOSDIS Land Processes Distributed Active Archive Center (LP DAAC), USGS Earth  
 136 Resources Observation and Science (EROS) Center, Sioux Falls, South Dakota, provided the MOD13A3 and  
 137 MCD12Q1 from the online Data Pool, accessible at <https://lpdaac.usgs.gov/tools/data-pool/>.

Table 1: Description of the satellite and reanalysis data used

Product	Sub-product	Variable	Spatial Resolution	Period	Units	Short Name
ERA5L		Precipitation	0.1°	1981-2023	mm	P
		Maximum temperature			°C	T <sub>max</sub>
		Minimum temperature			°C	T <sub>min</sub>
		Volumetric Soil Water Content at 1m			m <sup>3</sup> /m <sup>3</sup>	SM
ERA5L*	MOD13A3.061	Atmospheric Evaporative Demand	0.1°	1981-2023	mm	AED
MODIS		Normalized Difference Vegetation Index	1 km	2000-2023		NDVI
		land cover IGBP scheme		2001-2022		land cover

\*Calculated from maximum and minimum temperatures derived from ERA5L with Eq. 1.

138 For soil moisture, water supply, and water demand variables, we used ERA5L (ECMWF Reanalysis version  
 139 5 over land) (Muñoz-Sabater et al., 2021), a reanalysis dataset that provides the evolution of atmospheric and

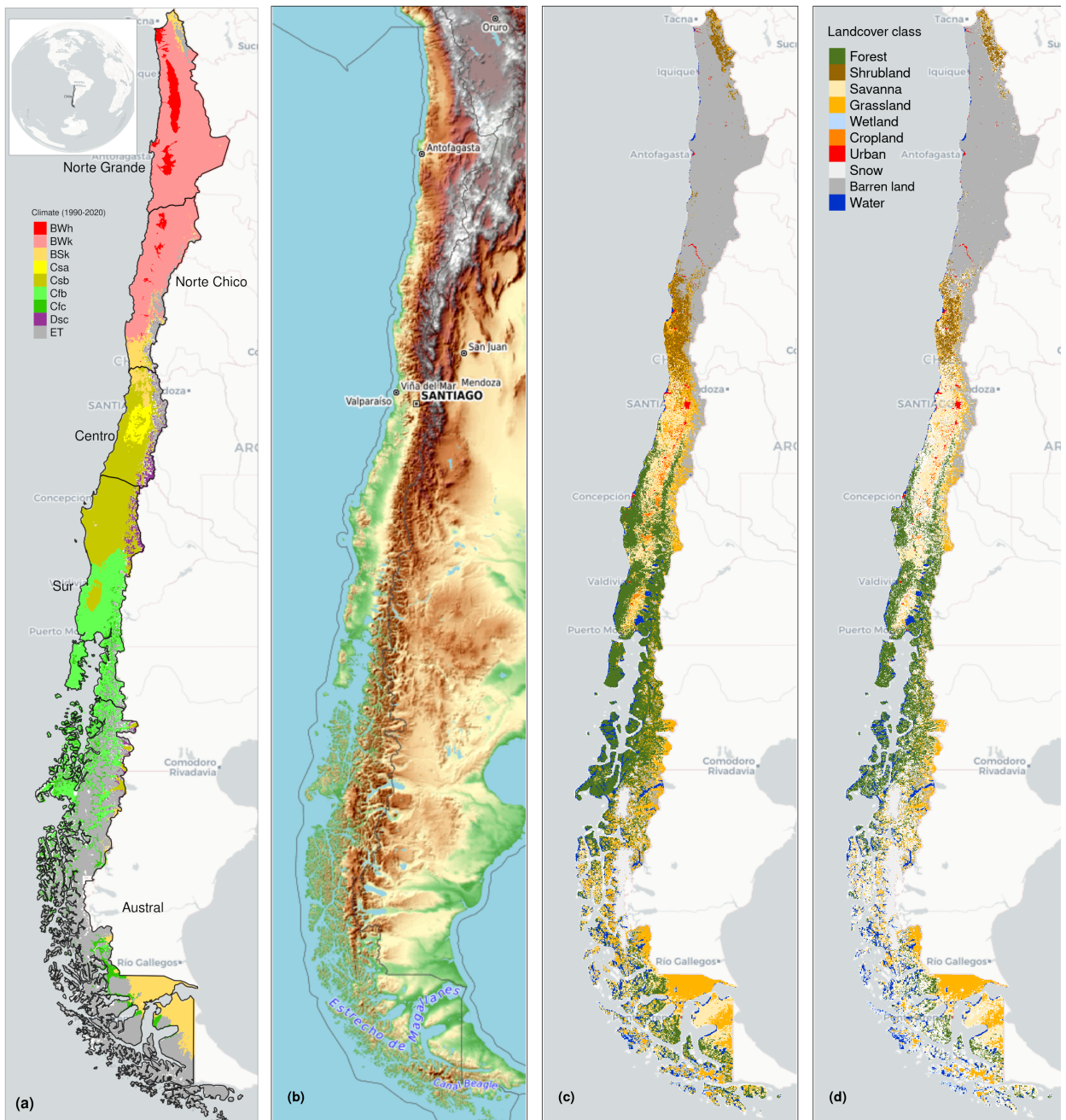


Figure 1: (a) Chile with the Koppen-Geiger climate classes and the five macrozones “Norte Grande”, “Norte Chico”, “Centro”, “Sur”, and “Austral”. (b) Topography reference map. (c) land cover classes for 2022. (d) Persistent land cover classes (> 80%) for 2001-2022

140 land variables since 1950. It has a spatial resolution of  $0.1^\circ$  (9 km), hourly frequency, and global coverage.  
 141 We selected the variables for total precipitation, maximum and minimum temperature at 2 meters, and  
 142 volumetric soil water layers between 0 and 100cm of depth (layer 1 to layer 3). Table 1 shows a summary  
 143 of the data and its main characteristics.

144 3.2. Short- to long-term drought trends

145 3.2.1. Atmospheric Evaporative Demand (AED)

146 In order to compute the drought indices that use water demand, it is necessary to first calculate the  
147 AED. To do this, we employed the Hargreaves method ([Hargreaves, 1994; Hargreaves and Samani, 1985](#)) by  
148 applying the following equation:

$$AED = 0.0023 \cdot Ra \cdot (T + 17.8) \cdot (T_{max} - T_{min})^{0.5} \quad (1)$$

149 where  $Ra$  ( $MJ\ m^2\ day^{-1}$ ) is extraterrestrial radiation;  $T$ ,  $T_{max}$ , and  $T_{min}$  are mean, maximum, and  
150 minimum temperature ( $^{\circ}C$ ) at 2m. For calculating  $Ra$  we used the coordinate of the latitud of the centroid  
151 of each pixel. We chose the method of Hargreaves to estimate AED because of its simplicity, which only  
152 requires temperatures and extrarrestrial radiation. Also, it has been recommended over other methods (e.g.,  
153 Penman-Monteith) when the access to climatic variables is limited ([Vicente-Serrano et al., 2014](#)).

154 3.2.2. Non-parametric calculation of drought indices

155 To derive the drought indices of water supply and demand, soil moisture, and vegetation (i.e., the proxy  
156 of productivity), we used the ERA5L dataset and the MODIS product, with a monthly frequency for 1981–  
157 2023 and 2000–2023, respectively. The drought indices correspond to a historical anomaly with regard to  
158 a variable (e.g., meteorological, vegetation, or soil moisture). To account for the anomaly, the common  
159 practice is to derive it following a statistical parametric methodology in which it is assumed that the  
160 statistical distribution of the data is known ([Heim, 2002](#)). A wrong decision is usually the highest source of  
161 uncertainty ([Laimighofer and Laaha, 2022](#)). In the case of Chile, due to its high degree of climatic variability,  
162 it is complex to choose a proper distribution without previous research. Here, we follow a non-parametric  
163 methodology for the calculation of the drought indices, in a similar manner as the framework proposed by  
164 [Farahmand and AghaKouchak \(2015\); Hobbins et al. \(2016\); McEvoy et al. \(2016\)](#).

165 For the purpose of monitoring water supply drought, we used the well-known Standardized Precipitation  
166 Index (SPI), which relies on precipitation data. To evaluate water demand, we chose the Evaporative  
167 Demand Drought Index (EDDI), developed by [Hobbins et al. \(2016\)](#) and [McEvoy et al. \(2016\)](#), which is based  
168 on the AED. The United States currently monitors drought using the EDDI (<https://psl.noaa.gov/eddi/>) as  
169 an experimental index. To consider the combined effect of water supply and demand, we selected the SPEI  
170 ([Vicente-Serrano et al., 2010](#)). For SPEI, an auxiliary variable  $D = P - AED$  is calculated. Soil moisture  
171 is the main driver of vegetation productivity, particularly in semi-arid regions ([Li et al., 2022](#)). Hence,  
172 for soil water drought, we used the SSI (Standardized Soil Moisture Index) ([Hao and AghaKouchak, 2013;](#)  
173 [AghaKouchak, 2014](#)). In our case, for the SSI, we used the average soil moisture from ERA5L at 1m depth.  
174 Finally, for the proxy of productivity, we used the zcNDVI proposed by [Zambrano et al. \(2018\)](#), which was  
175 derived from the monthly time series of NDVI derived from MOD13A1. All the indices are multi-scalar and  
176 can be used for the analysis of short- to long-term droughts.

177 To derive the drought indices, first we must calculate the sum of the variables with regard to the time scale  
178 (s). In this case, for generalization purposes, we will use  $V$ , referring to variables  $P$ ,  $AED$ ,  $D$ ,  $NDVI$ , and  
179  $SM$  (Table 1). We cumulated each  $V$  over the time series of  $n$  values (months), and for the time scales  $s$ :

$$A_{si} = \sum_{i=n-s-i+2}^{n-i+1} V_i \quad \forall i \geq n - s + 1 \quad (2)$$

180 The  $A_{si}$  corresponds to a moving window (convolution) that sums the variable for time scales  $s$  from  
181 the last month, month by month, until the first month in which it could sum for  $s$  months. An inverse  
182 normal approximation ([Abramowitz and Stegun, 1968](#)) obtains the empirically derived probabilities once

183 the variable cumulates over time for the scale  $s$ . Then, we used the empirical Tukey plotting position (Wilks,  
184 2011) over  $A_i$  to derive the  $P(A_i)$  probabilities across a period of interest:

$$P(A_i) = \frac{i - 0.33}{n + 0.33} \quad (3)$$

185 The drought indices *SPI*, *SPEI*, *EDDI*, *SSI*, and *zcNDVI* are obtained following the inverse normal  
186 approximation:

$$DI(A_i) = W - \frac{C_0 + C_1 \cdot W + c_2 \cdot W^2}{1 + d_1 \cdot W + d_2 \cdot W^2 + d_3 \cdot W^3} \quad (4)$$

187  $DI$  is referring to the drought index calculated for the variable  $V$  (i.e., SPI, SPEI, EDDI, SSI, and zcNDVI).  
188 The values for the constats are:  $C_0 = 2.515517$ ,  $C_1 = 0.802853$ ,  $C_2 = 0.010328$ ,  $d_1 = 1.432788$ ,  $d_2 =$   
189  $0.189269$ , and  $d_3 = 0.001308$ . For  $P(A) \leq 0.5$ ,  $W = \sqrt{-2 \cdot \ln(P(A_i))}$ , and for  $P(A_i) > 0.5$ , replace  $P(A_i)$   
190 with  $1 - P(A_i)$  and reverse the sign of  $DI(A_i)$ .

191 The drought indices were calculated for time scales of 1, 3, 6, 12, 24, and 36 months at a monthly frequency  
192 for 1981–2023 in order to be used for short- to long-term evaluation of drought. In the case of the proxy of  
193 vegetation productivity (zcNDVI), it was calculated for a time scale of six months at monthly frequency for  
194 2000–2023. For zcNDVI, we test time scales of 1, 3, 6, and 12 months in December and their correlation  
195 with net primary production (NPP) obtained from the MOD17A3HGF product from MODIS. We choose to  
196 use six months because r-squared with NPP increases from one to six months and from six to 12 months has  
197 little improvement. The r-squared were between 0.31 for forest and 0.72 for shrubland (see supplementary  
198 material in Section S5).

### 199 3.2.3. Trend of drought indices

200 To estimate if there are significant positive or negative trends for the drought indices, we used the non-  
201 parametric test of Mann-Kendall (Kendall, 1975). To determine the magnitude of the trend, we used Sen's  
202 slope (Sen, 1968). Some of the advantages of applying this methodology are that the Sen's slope is not  
203 affected by outliers as regular regression does, and it is a non-parametric method that is not influenced by  
204 the distribution of the data. We applied Mann-Kendall to see if the trend was significant and Sen's slope  
205 to estimate the magnitude of the trend. We did this to the six time scales from 1981 to 2023 (monthly  
206 frequency) and the indices SPI, EDDI, SPEI, and SSI. Thus, we have trends per index and time scale (24 in  
207 total). Then, we extracted the trend aggregated by macrozone and per land cover persistent macroclasses.

### 208 3.3. Interaction of land cover and drought

#### 209 3.3.1. Land cover change

210 To analyze the land cover change, we use the IGBP scheme from the MCD12Q1 collection 6.1 from MODIS.  
211 This product has been previously used for studies of drought and land cover in Chile (Fuentes et al., 2021;  
212 Zambrano et al., 2018). From the 17 classes, we regrouped into ten macroclasses, as follows: classes 1-4 to  
213 forest, 5-7 to shrublands, 8-9 to savannas, 10 as grasslands, 11 as wetlands, 12 and 14 to croplands, 13 as  
214 urban, 15 as snow and ice, 16 as barren, and 17 to water bodies. Thus, we have a land cover raster time series  
215 with the ten macroclasses for 2001 and 2023. We validate the land cover macroclasses regarding a highly  
216 detailed (30 m of spatial resolution) land cover map made for Chile by Zhao et al. (2016) for 2013-2014.  
217 Our results showed a global accuracy of ~0.82 and a F1 score of ~0.66. Section S2 in the Supplementary  
218 Material shows the procedure for validation.

219 We calculated the surface occupied per land cover class into the five macrozones (“Norte Grande” to  
220 “Austral”) per year for 2001–2023. After that, we calculated the trend’s change in surface per land cover

221 type and macroclass. We used Mann-Kendall for the significance of the trend (Kendall, 1975) and Sen's  
222 slope to calculate the magnitude (Sen, 1968).

223 Later in this study, we will examine the variation in vegetation productivity across various land cover  
224 types and how water demand and supply, and soil moisture affect it. In order to avoid variations due to a  
225 change in the land cover type from year-to-year that will wrongly impact NDVI, we developed a persistence  
226 mask for land cover for 2001–2022. Thereby, we reduce an important source of variation on a regional  
227 scale. Therefore, we generated a raster mask for IGBP MODIS per pixel using macroclasses that remained  
228 unchanged for at least 80% of the years (2001–2022). This enabled us to identify regions where the land  
229 cover macroclasses are persistent.

### 230 3.3.2. Relationship between land cover and drought trends

231 We wanted to explore the relationship between the trend in land cover classes and the trend in the drought  
232 indices. For this purpose, in order to have more representative results, we conducted the analysis over sub-  
233 basins within continental Chile. We use 469 basins, which have a surface area between 0.0746 and 24,000  
234 ( $km^2$ ), and a median area of 1,249 ( $km^2$ ). For each basin, we calculate the relative trend per land cover  
235 type, considering the proportion of the type relative to the total surface of the basin. Then, we extracted  
236 per basin the average trend of the drought indices SPI, SPEI, EDDI, SSI, and all their time scales 1, 3, 6,  
237 12, 24, and 36. Also, we extracted the average trend in the proxy of vegetation productivity (zcNDVI). We  
238 wanted to analyze which drought indices and time scales have a major impact on changes in land cover type.

239 We have 25 predictors, including drought indices and vegetation productivity. We analyzed the 25 predictors  
240 per type of landcover, thus running six random forest models. Random forest uses multiple decision  
241 trees and allows for classification and regression. Some advantages are that it allows to find no linear re-  
242 lationship, reduces overfitting, and allows to derive the variable importance. We used random forests for  
243 regression and trained 1000 forests. To obtain more reliable results, we resampled by creating ten folds,  
244 running a random forest per fold, and calculating the r-squared (rsq), root mean square error (RMSE), and  
245 variable importance.

246 The variable importance helps for a better understanding of the relationships by finding which variable has  
247 a higher contribution to the model. We calculate the variable's importance by permuting out-of-bag (OOB)  
248 data per tree and computing the mean standard error in the OOB. After permuting each predictor variable,  
249 we repeat the process for the resting variable. We repeated this process ten times (per fold) to obtain the  
250 performance metrics (rsq, RMSE, and variable importance).

### 251 3.4. Drought impacts on vegetation productivity

252 We analyzed the trend of vegetation productivity over the unchanged land cover macroclasses. To achieve  
253 this, we used the persistent mask of land cover macroclasses. This way, we tried to reduce the noise in the  
254 vegetation due to a change in land cover from year to year. We used the zcNDVI as a proxy of vegetation  
255 productivity. In Chile's cultivated land, Zambrano et al. (2018) introduced the zcNDVI for assessing seasonal  
256 biomass production in relation to climate.

257 We examine the drought indices of water demand, water supply, and soil moisture and their correlation  
258 with vegetation productivity. The objective is to determine the impact of soil moisture and water demand  
259 and supply on vegetation productivity. We want to address three main questions: Which of the drought  
260 variables—supply, demand, or soil moisture—most helps to explain the changes in plant productivity? How  
261 do the short- to long-term time scales of the drought variable affect vegetation productivity in Chile? And  
262 finally, how strong is the relationship between the variables and the drought index? Thus, we will be able to  
263 advance in understanding how climate is affecting vegetation, considering the impact on the five land cover  
264 types: forest, cropland, grassland, savanna, and shrubland.

265 We conducted an analysis on the linear correlation between the indices SPI, SPEI, EDDI, and SSI over  
266 time periods of 1, 3, 6, 12, 24, and 36 months with zcNDVI. We used a method similar to that used by

267 Meroni et al. (2017) which compared the SPI time-scales with the cumulative FAPAR (Fraction of Absorbed  
268 Photosynthetically Active Radiation). We performed a pixel-to-pixel linear correlation analysis for each  
269 index within the persistent mask of land cover macroclasses. We first compute the Pearson coefficient of  
270 correlation for each of the six time scales. A time scale is identified as the one that attains the highest  
271 correlation ( $p < 0.05$ ). We then extracted the Pearson correlation coefficient corresponding to the time  
272 scales where the value peaked. As a result, for each index, we generated two raster maps: 1) containing  
273 the raster with values of the time scales and drought index that reached the maximum correlation, and 2)  
274 having the magnitude of the correlation obtained by the drought index at the time scales.

275 *3.5. Software*

276 For the downloading, processing, and analysis of the spatio-temporal data, we used the open source software  
277 for statistical computing and graphics, R (R Core Team, 2023). For downloading ERA5L, we used the  
278 `{ecmwfr}` package (Hufkens et al., 2019). For processing raster data, we used `{terra}` (Hijmans, 2023) and  
279 `{stars}` (Pebesma and Bivand, 2023). For managing vectorial data, we used `{sf}` (Pebesma, 2018). For the  
280 calculation of AED, we used `{SPEI}` (Beguería and Vicente-Serrano, 2023). For mapping, we use `{tmap}`  
281 (Tennekes, 2018). For data analysis and visualization, the suite `{tidyverse}` (Wickham et al., 2019) was used.  
282 For the random forest modeling, we used the `{tidymodels}`(Kuhn and Wickham, 2020) and `{ranger}`(Wright  
283 and Ziegler, 2017) packages.

284 **4. Results**

285 *4.1. Short- to long-term drought trends*

286 Figure 2 shows the spatial variation of the trend for the drought indices from short- to long-term scales.  
287 SPI and SPEI have a decreasing trend from “Norte Chico” to “Sur.” However, there is an increasing trend  
288 in “Austral.” The degree of the trend is stronger at higher time scales. The SSI indicates that in “Norte  
289 Grande,” there are surfaces that have increased in the southwest part and in the northeast have decreased,  
290 and is shown for all time scales. Similar to SPI and SPEI, SSI decreases at higher time scales. EDDI showed  
291 a positive trend for the whole of continental Chile, with a higher trend toward the north and a descending  
292 gradient toward the south. The degree of trend increases at higher time scales.

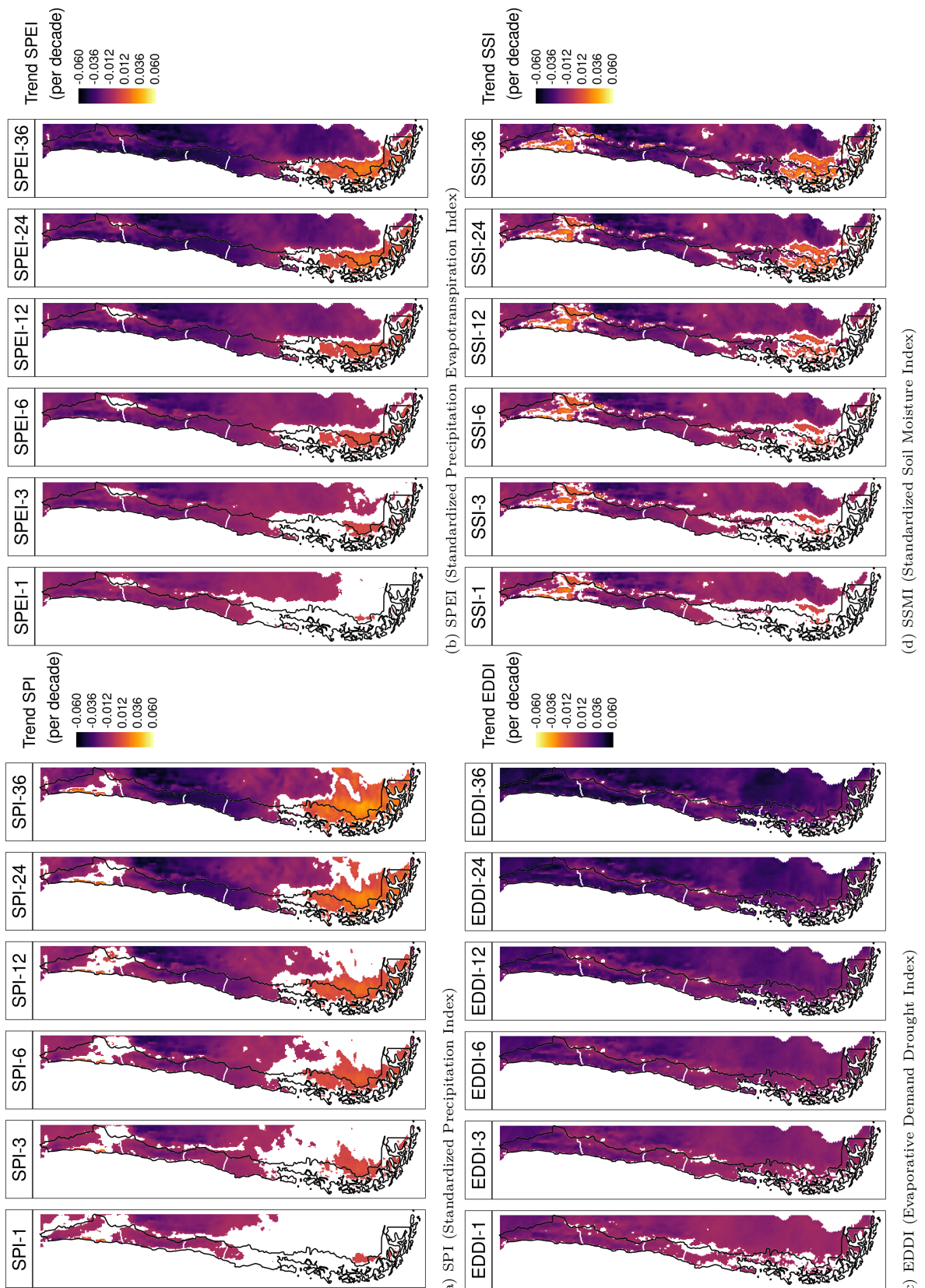


Figure 2: Linear trend of the drought index (\*) at time scales of 1, 3, 6, 12, 24, and 36 months for 1981-2023

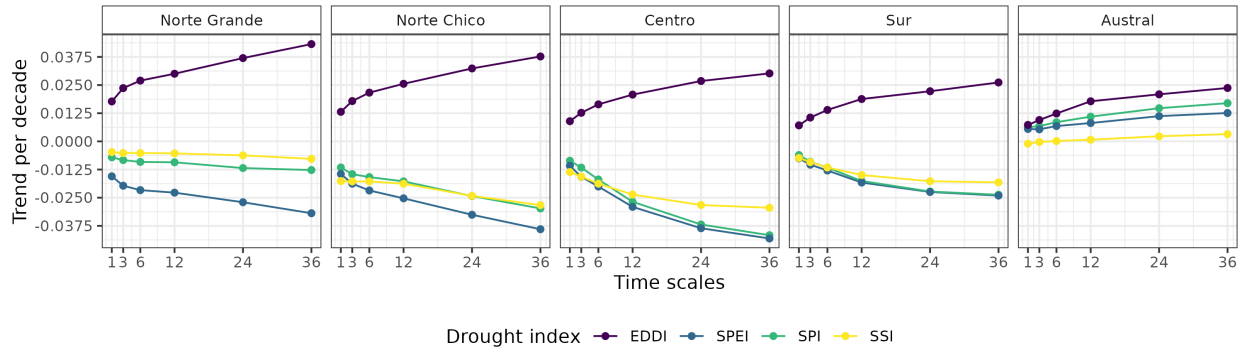


Figure 3: Trend per decade for the drought indices SPI, EDDI, SPEI, and SSI aggregated by macrozone.

293 The Figure 3 displays the averaged aggregation per macrozone, the drought index, and the timescale. The  
 294 macrozones that reached the lowest trend for SPI, SPEI, and SSI are “Norte Chico” and “Centro,” where  
 295 the indices also decrease at longer time scales. Potentially explained due to the prolonged reduction in  
 296 precipitation that has affected the hydrological system in Chile. At 36 months, it reaches trends between  
 297 -0.03 and -0.04 (z-score) per decade for SPI, SPEI, and SSI. For “Sur,” the behavior is similar, decreasing  
 298 at longer scales and having between -0.016 and -0.025 per decade for SPI, SPEI, and SSI. “Norte Grande”  
 299 has the highest trend at 36 months for EDDI (0.042 per decade), and “Centro” has the lowest for SPI and  
 300 SPEI. In “Norte Grande” and “Norte Chico,” which are in a semi-arid climate, it is evident that the EDDI  
 301 has an effect on the difference between the SPI and SPEI index, which is not seen in the other macrozones.  
 302 Contrary to the other macrozones, “Austral” showed an increase in all indices, being the highest for EDDI  
 303 at 36 months (0.025) and the lowest for SSI, which shows only a minor increase in the trend.

#### 304 4.2. Interaction of land cover and drought

##### 305 4.2.1. Land cover change

Table 2: Surface of the land cover class that persist during 2001-2022

macrozone	Surface [km <sup>2</sup> ]					
	Forest	Cropland	Grassland	Savanna	Shrubland	Barren land
Norte Grande			886		7,910	171,720
Norte Chico		90	4,283	589	16,321	84,274
Centro	3,739	1,904	7,584	19,705	844	12,484
Sur	72,995	1,151	7,198	15,906		2,175
Austral	60,351		54,297	19,007	249	7,218
Total	—	137,085	3,145	74,247	55,206	25,324
						277,870

306 For vegetation, we obtained and use hereafter five macroclasses of land cover from IGBP MODIS: forest,  
 307 shrubland, savanna, grassland, and croplands. Figure 1c shows the spatial distribution of the macroclasses  
 308 through Chile for the year 2022. Figure 1d shows the macroclasses of land cover persistance (80%) during  
 309 2021–2022, respectively (Table 2). Within continental Chile, barren land is the land cover class with the  
 310 highest surface area ( $277,870 \text{ km}^2$ ). The largest type of vegetation, with  $137,085 \text{ km}^2$ , is forest. Grassland  
 311 has  $74,247 \text{ km}^2$ , savanna  $55,206 \text{ km}^2$ , shrubland  $25,341 \text{ km}^2$ , and cropland  $3,146 \text{ km}^2$  (Table 2). The  
 312 macrozones with major changes for 2001–2022 were “Centro,” “Sur,” and “Austral,” with 36%, 31%, and  
 313 34% of their surface changing the type of land cover, respectively (Figure 1 and Table 3). Figure 4 shows  
 314 the summary of the proportion of surface per land cover class and macrozone, derived from the persistance  
 315 mask over continental Chile.

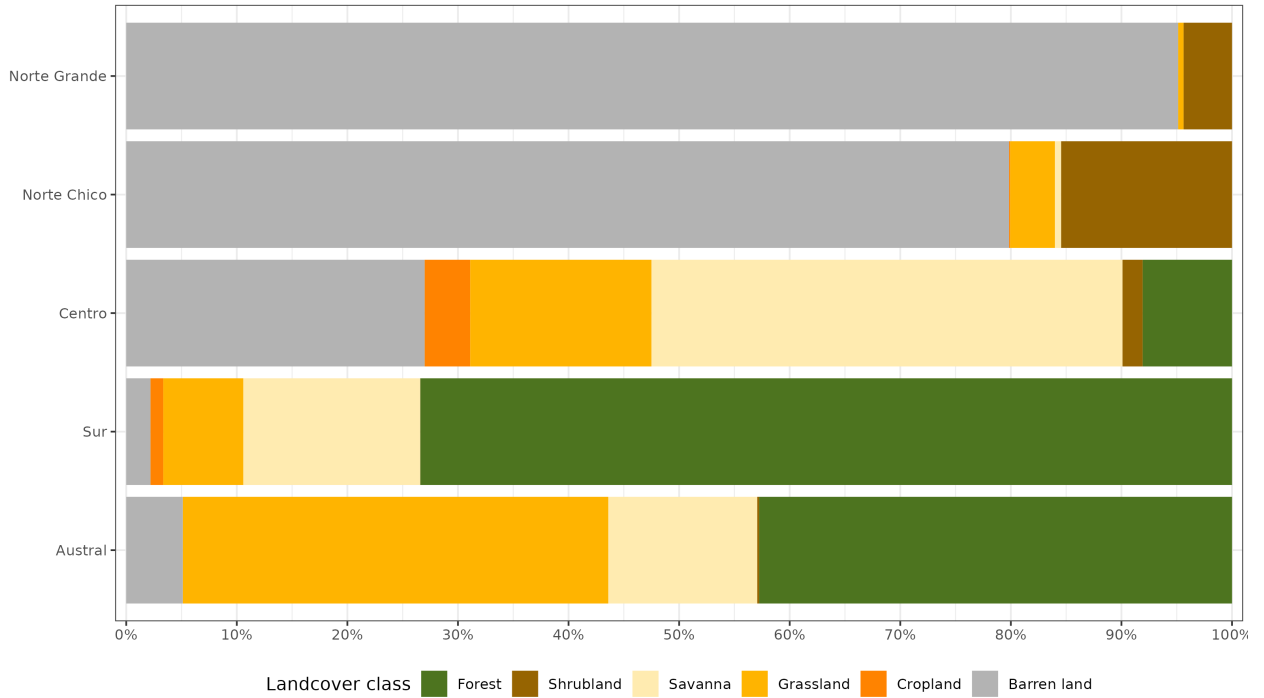
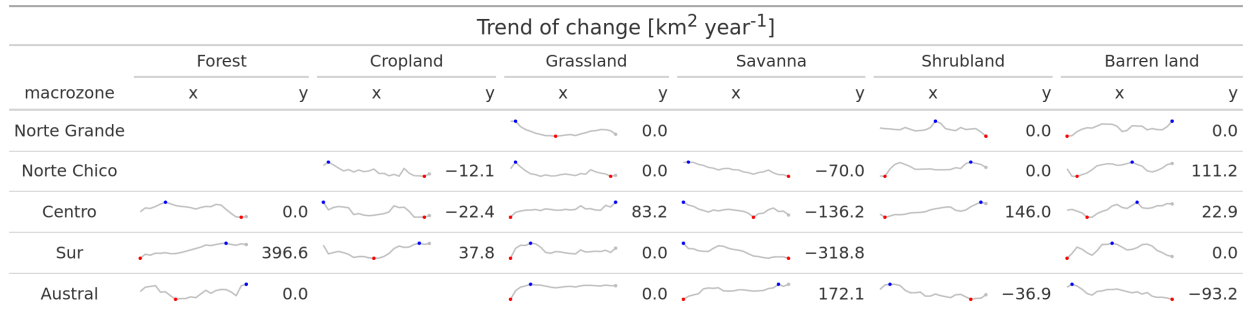


Figure 4: Proportion of land cover class from the persistent land cover for 2001-2022 (>80%) per macrozone

Table 3: The value of Sen's slope trend next to the time-series plot of surface per land cover class (IGBP MCD12Q1.016) for 2001–2022 through Central Chile. Values of zero indicate that there was not a significant trend. Red dots on the plots indicate the maximum and minimum values of surface.



From the trend analysis in Table 3, we can indicate that the “Norte Chico” shows an increase in barren land of  $111 \text{ km}^2 \text{ yr}^{-1}$  and a reduction in the class savanna of  $70 \text{ km}^2 \text{ yr}^{-1}$ . In the “Centro” and “Sur,” there are changes with an important reduction in savanna ( $136$  to  $318 \text{ km}^2 \text{ yr}^{-1}$ ), and an increase in shrubland and grassland. Showing a change for more dense vegetation types. The area under cultivation (croplands) appears to be shifting from the “Centro” to the “Sur.” Also, there is a high increase in forest ( $397 \text{ km}^2 \text{ yr}^{-1}$ ) in the “Sur,” seemingly replacing the savanna lost (Table 3).

#### 4.2.2. Relationship between drought indices and land cover change

According to Table 4, the random forest models for estimating the landcover trend from the trends in drought indices reach an r-squared between 0.32 and 0.39 for the types of forest, grassland, savanna, shrubland, and barren land. It is more likely that short- and medium-term increases in AED (EDDI-6 and

Table 4: The five most important trends of drought indices in estimating the landcover trend per land cover type and the r-squared (rsq) reached by each random forest model.

Position	Forest (rsq=0.32)	Cropland (rsq=0.06)	Grassland (rsq=0.39)	Savanna (rsq=0.23)	Shrubland (rsq=0.23)	Barren_land (rsq=0.32)
1	EDDI-36	EDDI-36	EDDI-6	EDDI-6	EDDI-6	EDDI-12
2	EDDI-24	SSI-36	EDDI-12	EDDI-12	SPI-36	EDDI-6
3	EDDI-12	EDDI-24	EDDI-24	SPI-36	SPEI-36	SPI-6
4	SSI-36	EDDI-12	SPEI-6	EDDI-36	EDDI-3	SPEI-6
5	SSI-6	SSI-24	SPI-6	EDDI-24	SPI-24	EDDI-24

326 EDDI-12) and short-term precipitation deficits (SPI-6 and SPEI-6) contributed to changes in grassland and  
 327 bare land. The short-term increase of AED (EDDI-3 and EDDI-6) and the longer duration of the precipitation  
 328 deficit (SPI-24, SPI-36, and SPEI-36) most likely contribute to the changes in shrubland. The changes  
 329 in savanna are associated with a short- and long-term increase in AED and a three-year precipitation deficit  
 330 (SPI-36). The increase in cumulative AED from 12 to 36 months is the strongest associated variable that  
 331 contributes to changes in forests, followed by the reduction of soil moisture over six and 36 months. The  
 332 supplementary material in Section S3 provides further details about the variable's importance.

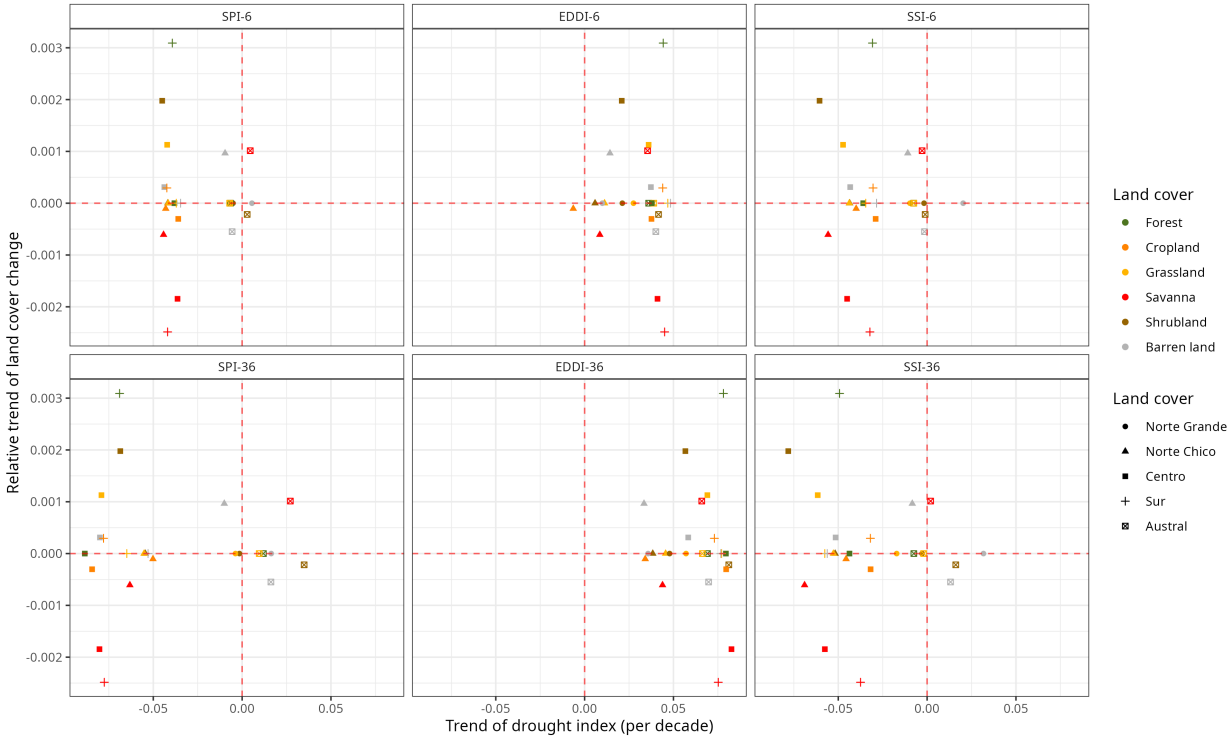


Figure 5: Relationship between the trend in land cover change (y-axis) and the trend in drought indices (x-axis) for the five macrozones. Vertical panels correspond to 1, 3, 6, 12, 24, and 36 months of the time scale by drought index. Horizontal panels show each drought index

333 We study the connection between the SPI, EDDI, and SSI drought indices and changes in land cover in  
 334 Figure 5. To do this, we compare the relative changes in land cover (in terms of the total surface area per

335 land cover type and macrozone) over six and thirty-six months. Figure 5 shows that the forest in the “Sur,”  
 336 shrubland and grassland in “Centro,” barren land in “Norte Chico,” and savanna in “Austral” showed an  
 337 increase in the surface of landcover associated with an increase in EDDI. Savanna in “Centro,” “Sur,” and  
 338 “Norte Chico” decreases with the increase in EDDI. The SPI and SSI showed similar behavior regarding  
 339 the trend in land cover type. A decrease in SPI and SSI is associated with an increase in the surface in  
 340 shrubland and grassland in “Centro,” forest in “Sur,” and barren land in “Norte Chico,” as well as a  
 341 decrease trend in savanna in “Norte Chico,” “Centro,” and “Sur.”

#### 342 4.3. Drought impacts on vegetation productivity within land cover

##### 343 4.3.1. Trends in vegetation productivity



Figure 6: (a) Map of the linear trend of the index zcNDVI for 2000–2023. Greener colors indicate a positive trend; redder colors correspond to a negative trend and a decrease in vegetation productivity. Grey colors indicate either no vegetation or a change in land cover type for 2001–2022. (b) Temporal variation of zcNDVI aggregated at macrozone level within continental Chile. Each horizontal panel corresponds to a macrozone from ‘Norte Grande’ to ‘Austral’.

344 The temporal variation within the macrozones is shown in Figure 6b). There is a negative trend in “Norte  
 345 Chico” with -0.035 and “Centro” with -0.02 per decade. Vegetation reached its lowest values for 2019-2022,  
 346 with an extreme condition in early 2020 and 2022 in the “Norte Chico” and “Centro”. The “Sur” and  
 347 “Austral” show a positive trend of around 0.012 and 0.016, respectively, per decade (Figure 6).

348 In Figure 6 it is showed the spatial map of trends in zcNDVI (Figure 6a). In “Norte Grande,” vegetation  
 349 productivity, as per the z-index, exhibits a yearly increase of 0.027 for grassland and 0.032 for shrubland. In  
 350 the “Norte Chico,” savanna has the lowest trend of -0.062, cropland -0.047, shrubland -0.042, and grassland  
 351 -0.037. In “Centro,” shrubland reaches -0.07, savanna -0.031, cropland -0.024, forest -0.017, and grassland  
 352 -0.005 per decade. This decrease in productivity could be associated either with a reduction in vegetation  
 353 surface, a decrease in biomass, or browning.

##### 354 4.3.2. Correlation between vegetation productivity and drought indices

355 Figure 7 shows the highest coefficient of determination ( $r^2$ , or rsq) found in the regression analysis  
 356 between zcNDVI and different drought indicators over time scales of 1, 3, 6, 12, 24, and 36 months. The  
 357 spatial variation of time scales reached per index is mostly for time scales above 12 months. In the case of  
 358 SSI, the predominant scales are 6 and 12 months. For all indices, to the north, the time scales are higher

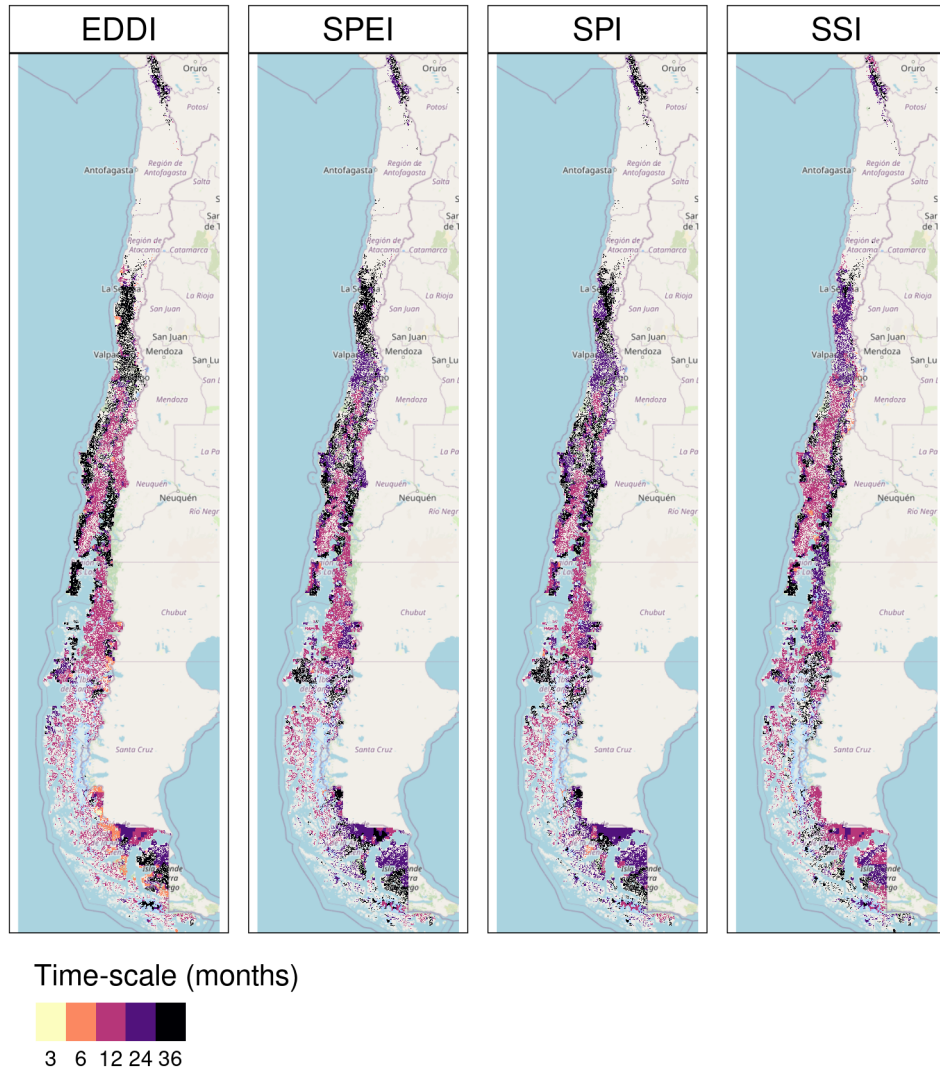


Figure 7: Time scales per drought index that reach the maximum coefficient of determination

and diminish toward the south until the south part of “Austral,” where they increase. In Figure 8, the map of Pearson correlation values ( $r$ ) is shown. The EDDI reached correlations above 0.5 between “Norte Chico” and “Sur.” The correlation changes from negative to positive toward the Andes Mountains and to the sea, just as in the northern part of “Austral.” The SPI and SPEI have similar results, with the higher values in “Norte Chico” and “Centro” being higher than 0.6. Following a similar spatial pattern as EDDI but with an opposite sign. The SSI showed to be the index that has a major spatial extension with a higher correlation. It has a similar correlation to SPI and SPEI for “Norte Chico” and “Sur,” but has improvements for “Sur.”

In Table 5, we aggregate per macrozone and landcover the correlation analysis presented in Figure 7 and Figure 8. According to what is shown, forests seem to be the most resistant to drought. Showing that only “Centro” is slightly ( $rsq = 0.25$ ) impacted by a 12-month soil moisture deficit (SSI-12). In the “Norte Chico” and to a lesser extent in the “Norte Grande,” it is evident that a SSI-12 with a  $rsq = 0.45$  and a decrease in water supply (SPI-36 and SPEI-24 with  $rsq = 0.28$  and 0.34, respectively) have an impact on grasslands. However, this type was unaffected by soil moisture, water supply, or demand in macrozones further south. The types that show to be most affected by variation in climate conditions are shrublands,

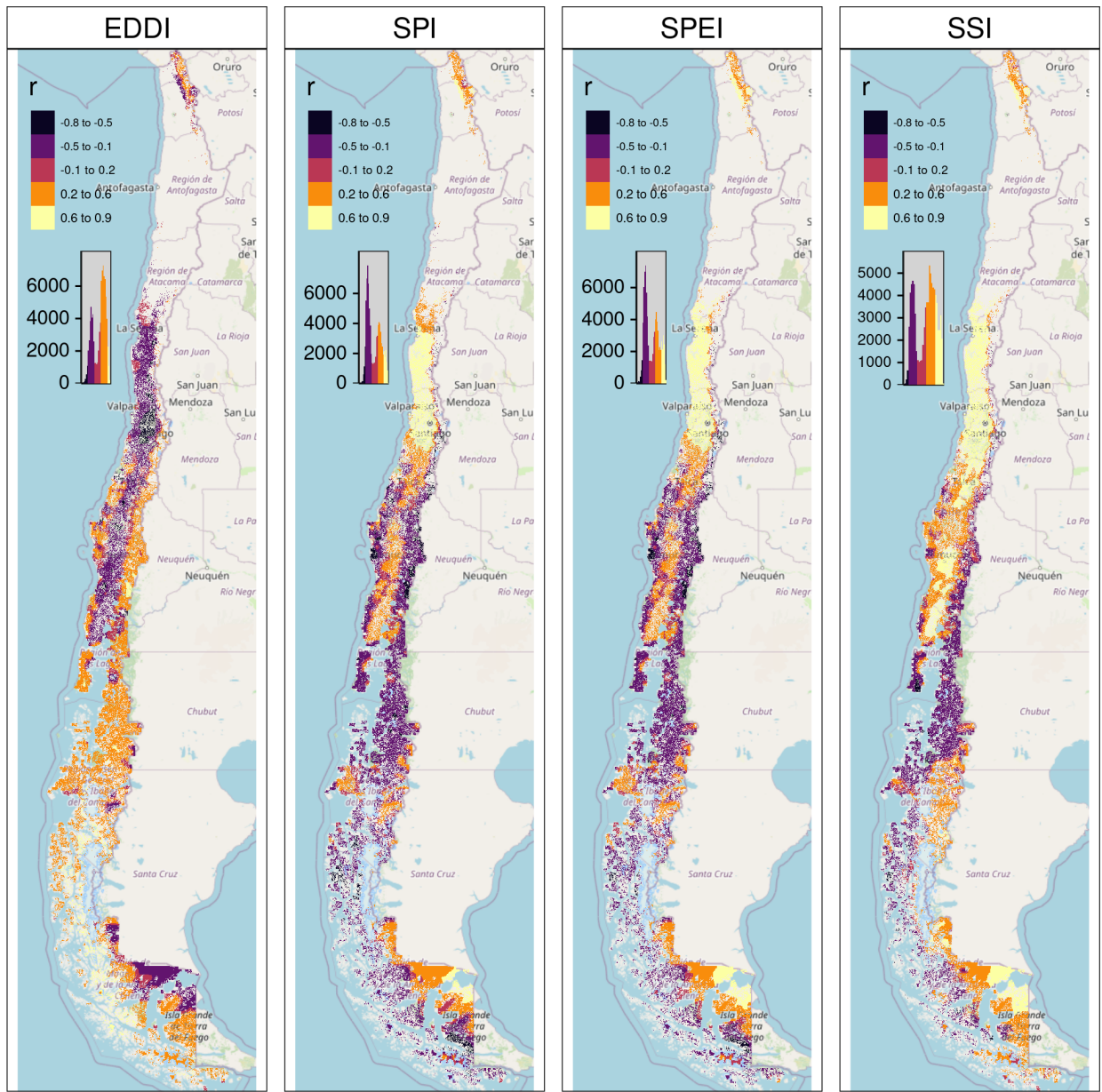
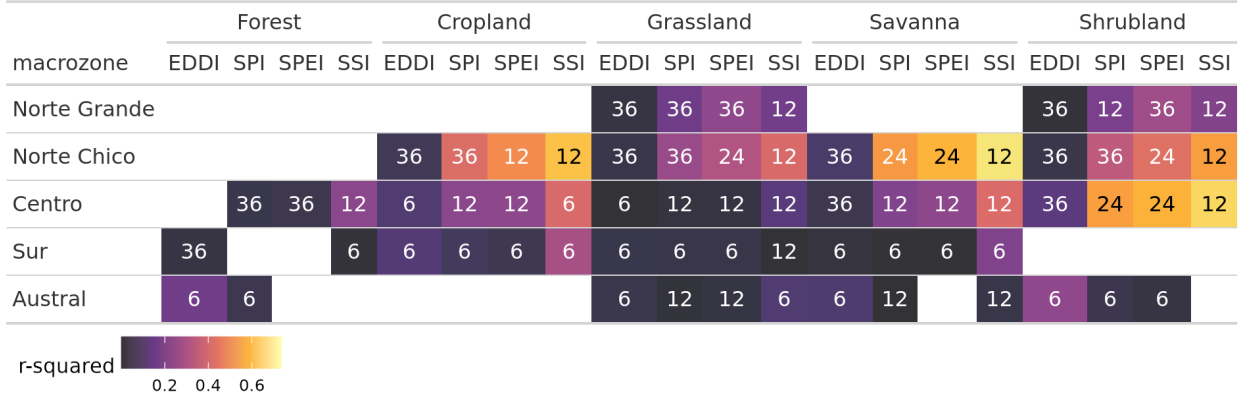


Figure 8: Pearson correlation value for the time scales and drought index that reach the maximum coefficient of determination

373 savannas, and croplands. For savannas in “Norte Chico,” the SSI-12 and SPI-24 reached an rsq of 0.74  
 374 and 0.58, respectively. This value decreases to the south, but the SSI-12 is still the variable explaining  
 375 more of the variation in vegetation productivity (rsq = 0.45 in “Centro” and 0.2 in “Sur”). In the case  
 376 of croplands, the SPEI-12, SPI-36, and SSI-12 explain between 45% and 66% of the variability in “Norte  
 377 Chico.” The type of land most impacted by climatic variation was shrubland, where soil moisture explained  
 378 59% and precipitation, 37%, in “Norte Chico” and “Centro,” with SSI-12 being the most relevant variable,  
 379 then SPI-36 in “Norte Chico” and SPI-24 in “Sur.”

Table 5: Summary per land cover macroclass and macrozone regarding the correlation between zcNDVI with the drought indices EDDI, SPI, SPEI, and SSI for time scales of 1, 3, 6, 12, 24, and 36. The numbers in each cell indicate the time scale that reached the maximum correlation for the land cover and macrozone, and the color indicates the strength of the r-squared obtained with the index and the time scale.



## 380 5. Discussion

### 381 5.1. The main drivers of drought in Chile

382 Vicente-Serrano et al. (2022), in a study at the global scale of drought trends, indicates that there have  
 383 not been significant trends in meteorological drought since 1950. Also, state that the increase in hidrological  
 384 trend in some parts of the globe (northeast Brazil and the Mediterranean region) is related to changes  
 385 in land cover and specifically to the rapidly increasing irrigated area, which consequently increases water  
 386 extraction. Kogan et al. (2020) analyzed the agricultural drought impact globally and in the main grain  
 387 producer countries, finding that “since 1980, the Earth warming has not changed the drought area or  
 388 intensity.” In our study, we took into account the variation in vegetation productivity in Chile, specifically  
 389 in areas without any changes in land cover, to prevent any misleading conclusions about the increase in water  
 390 demand due to land cover change. Our results show a contrasting perspective. The SPI, SPEI, and SSI  
 391 (water supply) showed a decrease in trends, except for the southern part, and an increase in EDDI (water  
 392 demand). The trend, positive or negative, was stronger as the time scales increased. Trends in the long  
 393 term (e.g., 36 months) are evidence of how human-induced climate change is affecting Chile, which seems  
 394 to be due to an intense hydrological drought resulting from the persistence of the precipitation deficit. We  
 395 found that there has been a significant trend in the decline of vegetation productivity (zcNDVI) since 2000  
 396 for the north-central part of the country, which has been extreme between 2020 and 2022 and has impacted  
 397 natural and cultivated land. Additionally, we demonstrated that the drought, primarily due to an increase  
 398 in AED, accounts for about 30% of the changes in land cover types (excluding croplands). These changes  
 399 are associated with a decrease in water demand from vegetation. Moreover, the most water-demanding  
 400 type, cropland, showed a decrease in the north-central region, while barren land showed an increase. The  
 401 north-central part of the country primarily experienced these changes due to a higher increase in AED.  
 402 Thus, we have evidence of a significant decline in water supply and an increase in AED for the north-central  
 403 part of Chile, which show to be the most relevant variables for drought conditions. Some questions arise  
 404 regarding what is occurring with the cultivated land. We used the unchanged land cover to ensure that an  
 405 increase in surface area is not considered in the trend analysis. For croplands, it could happen that some  
 406 areas have changed the types of crops for others with higher water demand, which consequently increases  
 407 water demand. However, this effect should be minor compared to the decrease in water supply and increase  
 408 in water demand at this scale of analysis.

409 This shows that the main cause of the hydrological drought in Chile was a steady drop in water supply  
 410 made worse by an increase in AED, but it seems that in zones most affected by drought, the main cause is

411 not an increase in vegetation water demand due to an intensification of cultivated land (e.g., an increase in  
412 irrigated crops). North-central Chile has experienced a decline in vegetation productivity across land cover  
413 types, which is primarily attributable to variations in water supply and soil moisture. An increase in water  
414 demand, such as an increase in the surface area of irrigated crops, could strengthen this trend. But it is out  
415 of the scope of this study. Future work should focus on the regions where the drought has been more severe  
416 and has a high proportion of irrigated crops to get insight on the real impact of irrigation on those zones.

417 *5.2. Land cover sensitivity to drought*

418 We analyzed two main impacts of drought on land cover. First, the attribution of drought to the change  
419 in surface area per land cover type. Drought accounts for about 30% of the surface change per land cover  
420 type, with the exception of croplands. The main variables associated with these changes are the increase  
421 in AED and, in second place, the decrease in precipitation. Second, we analyzed the time series of drought  
422 indices and vegetation productivity per land cover type. In this case, the most important variables that had  
423 an impact on zcNDVI were the soil moisture deficit, followed by the precipitation deficit, and in third place,  
424 AED.

425 In a study in the Yangtze River Basin in China, [Jiang et al. \(2020\)](#) analyzed the impact of drought on  
426 vegetation using the SPEI and the Enhanced Vegetation Index (EVI). They found that cropland was more  
427 sensitive to drought than grassland, showing that cropland responds strongly to short- and medium-term  
428 drought (< SPEI-6). In our case, the SPEI-12 was the one that most impacted the croplands in “Norte  
429 Chico” and “Centro.” In general, most studies show that croplands are most sensitive to short-term drought  
430 (< SPI-6) ([Zambrano et al., 2016](#); [Potopová et al., 2015](#); [Dai et al., 2020](#); [Rhee et al., 2010](#)). Short-term  
431 precipitation deficits impact soil water, and thus less water is available for plant growth. However, we  
432 found that in “Norte Chico,” an SPI-36 and SPEI-12 had a higher impact, which are associated with  
433 hydrological drought (long-term), and in “Centro,” an SPI-12 and SPEI-12. Thus, we attribute this impact  
434 to the hydrological drought that has decreased groundwater storage ([Tau care et al., 2024](#)), which in turn  
435 is impacted by long-term deficits, and consequently, the vegetation is more dependent on groundwater. In  
436 “Sur” and “Austral,” the correlations between drought indices and vegetation productivity decrease, as do  
437 the time scales that reach the maximum r-squared. The possible reason for this is that the most resistant  
438 types, forest and grassland, predominate south of “Centro.” Also, drought episodes have been less frequent  
439 and intense. The drought episodes have had a lower impact on water availability for vegetation.

440 According to [Senf et al. \(2020\)](#), severe drought conditions in Europe are a significant cause of tree mortality.  
441 However, we discovered that forests, as the most resilient land cover class to drought, experience less variation  
442 in drought indices. Supporting this is [Fathi-Taperasht et al. \(2022\)](#), who asserts that Indian forests are the  
443 most drought-resistant and recover rapidly. Similarly, the work of [Wu et al. \(2024\)](#), who analyzed vegetation  
444 loss and recovery in response to meteorological drought in the humid subtropical Pearl River basin in China,  
445 indicates that forests showed higher drought resistance. Using Vegetation Optical Depth (VOD), kNDVI,  
446 and EVI, [Xiao et al. \(2023\)](#) tests the resistance of ecosystems and finds that ecosystems with more forests  
447 are better able to handle severe droughts than croplands. They attribute the difference to a deeper rooting  
448 depth for trees, a higher water storage capacity, and different water use strategies between forest and  
449 cropland ([Xiao et al., 2023](#)). In contrast, [Venegas-González et al. \(2023\)](#), who studied *Cryptocarya alba* and  
450 *Beilschmiedia miersii* (both from the Lauraceae family) that live in sclerophyllous forests in Chile, found  
451 that the trees’ overall growth had slowed down. This could mean that the natural dynamics of their forests  
452 have changed. They attributed it to the cumulative effects of the unprecedented drought (i.e., hydrological  
453 drought).

454 Thus, we attribute that forest to being the most resistant to drought, due to the fact that most of the species  
455 comprising it are highly resilient to water scarcity compared to the other land cover classes. Nonetheless, if  
456 we want to go deep in our analysis, we should use earth observation data that is able to capture a higher  
457 level of detail. For example, when we used MOD13A3 with a 1km spatial resolution to measure vegetation  
458 condition, it took the average condition of 1 square kilometer. Then, to use remote sensing to look at how a

459 certain type of forest (like sclerophyllous forest) changes in response to drought on a local level, we should  
460 use operational products with higher spatial resolutions, like those from Landsat or Sentinel. This will let  
461 us do a more thorough analysis.

462 *5.3. Vegetation productivity and drought.*

463 We found that the 12-month soil moisture deficit most affects the productivity of vegetation in all land  
464 cover types along Chile. The main external factors that affect biomass production by vegetation are actual  
465 evapotranspiration and soil moisture, and the rate of ET in turn depends on the availability of water storage  
466 in the root zone. Thus, soil moisture plays a key role in land carbon uptake and, consequently, in the  
467 production of biomass (Humphrey et al., 2021). Moreover, Zhang et al. (2022) indicate there is a bidirectional  
468 causality between soil moisture and vegetation productivity. Lastly, some studies have redefined agricultural  
469 drought as soil moisture drought from a hydrological perspective (Van Loon et al., 2016; Samaniego et al.,  
470 2018). Even though soil moisture is the external factor most determinant of vegetation biomass, there  
471 are multiple internal factors, such as species, physiological characteristics, and plant hydraulics, that would  
472 affect vegetation productivity. Because of that, we believe that agricultural drought, referring to the drought  
473 that impacts vegetation productivity, is the most proper term, as originally defined by Wilhite and Glantz  
474 (1985).

475 The study results showed that the soil moisture-based drought index (SSI) was better at explaining vegeta-  
476 tion productivity across land cover macroclasses than meteorological drought indices like SPI, SPEI, and  
477 EDDI. In the early growing season and especially in irrigated rather than rainfed croplands, soil moisture  
478 has better skills than SPI and SPEI for estimating gross primary production (GPP). This according to  
479 Chatterjee et al. (2022) evaluation of the SPI and SPEI and their correlation with GPP in the CONUS.  
480 Also, Zhou et al. (2021) indicate that the monthly scaled Standardized Water Deficit Index (SWDI) can  
481 accurately show the effects of agricultural drought in most of China. Nicolai-Shaw et al. (2017) also looked  
482 at the time-lag between the SWDI and the Vegetation Condition Index (VCI). They found that there was  
483 little to no time-lag in croplands but a greater time-lag in forests.

484 In our case, there is strong spatial variability throughout Chile and between classes, mainly attributable to  
485 climate heterogeneity, hydrological status, or vegetation resistance to water scarcity. The semi-arid “Norte  
486 Chico” and the Mediterranean “Centro” were where SSI had the best performance. In Chile, medium-term  
487 deficits of 12 months are more relevant in the response of vegetation, which decreases to the south, and in the  
488 case of croplands, they seem to react in a shorter time, with six months (SSI-6) in “Centro.” This variation  
489 for croplands could be related to the fact that in “Norte Chico,” the majority of crops are irrigated, but  
490 to the south there is a higher proportion of rainfed agriculture, which is most dependent on the short-term  
491 availability of water. Rather, in the “Norte Chico,” the orchards are more dependent on the storage of water  
492 in dams of groundwater reservoirs, which are affected by long-term drought (e.g., SPI-36).

493 *5.4. Drought information to aid in adaptation*

494 Different climate components, such as evaporative water demand, water supply, soil moisture, and their  
495 impact on vegetation, should be considered when evaluating the multi-dimensional nature of drought. For  
496 a better understanding of the propagation of drought (Van Loon et al., 2012) from meteorological to hy-  
497 drological drought, we should consider the climatic response at different time scales, ranging from short to  
498 long. Furthermore, we must make this information publicly available and update it frequently to aid in  
499 the development of adaptation policies. The drought observatory for agriculture and biodiversity of Chile  
500 (ODES) shares this information aggregated for multiple administrative and hydrological units across Chile  
501 (<https://odes-chile.org/app/unidades>), with the goal of helping to prepare for future climatic conditions.

502    **6. Conclusion**

503    There is a trend toward decreasing water supply (SPI, SPEI, and SSI) in most of Chile; just in the southern  
504    part, there is an increase. The trend is most strong in the north-central zone. The whole country showed  
505    an increase in water demand (AED). The magnitude of the trend increases over longer time scales, which is  
506    evidence that the deficit is impacting the hydrological system in Chile. The trend in vegetation productivity  
507    in the north-central area is affecting, to a higher degree, shrubland and savanna, followed by croplands and  
508    forests. The most important changes in land cover are the increase of forest in “Sur” and shrubland and  
509    grassland in “Centro;” and the increase of savanna in “Centro” and “Sur.”

510    The drought explains about 30% of the change in land cover type across Chile for forest, grassland,  
511    shrubland, and savanna. There is no evidence of an effect of drought on the change in cropland surface area.  
512    The increase in AED is the main driver of the change in land cover, followed by a reduction in precipitation  
513    and soil moisture. The drought time scales vary regarding the land cover type.

514    The change in vegetation productivity has been severe in the north-central part of the country for all land  
515    cover types, particularly savanna, shrubland, and croplands. The anomaly in soil moisture over the past 12  
516    months is the main variable explaining these changes, followed by anomalies in cumulated precipitation over  
517    one to two years. The variation in AED seems to intensify the drought impact on vegetation productivity.

518    The results of this study provide insightful information that would help in developing adaptation measures  
519    for ecosystems in Chile to cope with climate change and drought.

520    **7. Acknowledgment**

521    The National Research and Development Agency of Chile (ANID) funded this study through the drought  
522    emergency project FSEQ210022, Fondecyt Iniciación N°11190360, and Fondecyt Regular N°1210526.

523    **References**

- 524    Abramowitz, M., Stegun, I.A., 1968. Handbook of mathematical functions with formulas, graphs, and mathematical tables. volume 55. US Government printing office.
- 525    Aceituno, P., Boisier, J.P., Garreaud, R., Rondanelli, R., Rutllant, J.A., 2021. Climate and Weather in Chile, in: Fernández, B., Gironás, J. (Eds.), Water Resources of Chile. Springer International Publishing, Cham. volume 8, pp. 7–29. URL: [http://link.springer.com/10.1007/978-3-030-56901-3\\_2](http://link.springer.com/10.1007/978-3-030-56901-3_2).
- 526    AghaKouchak, A., 2014. A baseline probabilistic drought forecasting framework using standardized soil moisture index: application to the 2012 United States drought. *Hydrology and Earth System Sciences* 18, 2485–2492. URL: <https://hess.copernicus.org/articles/18/2485/2014/>, doi:10.5194/hess-18-2485-2014.
- 527    AghaKouchak, A., Mirchi, A., Madani, K., Di Baldassarre, G., Nazemi, A., Alborzi, A., Anjileli, H., Azarderakhsh, M., Chiang, F., Hassanzadeh, E., Huning, L.S., Mallakpour, I., Martinez, A., Mazdiyasni, O., Moftakhari, H., Norouzi, H., Sadegh, M., Sadeqi, D., Van Loon, A.F., Wanders, N., 2021. Anthropogenic Drought: Definition, Challenges, and Opportunities. *Reviews of Geophysics* 59, e2019RG000683. URL: <https://agupubs.onlinelibrary.wiley.com/doi/10.1029/2019RG000683>, doi:10.1029/2019RG000683.
- 528    Akinyemi, F.O., 2021. Vegetation Trends, Drought Severity and Land Use-Land Cover Change during the Growing Season in Semi-Arid Contexts. *Remote Sensing* 2021, Vol. 13, Page 836 13, 836. URL: <https://www.mdpi.com/2072-4292/13/5/836/>, doi:10.3390/RS13050836. publisher: Multidisciplinary Digital Publishing Institute.
- 529    Bakker, K., 2012. Water Security: Research Challenges and Opportunities. *Science* 337, 914–915. URL: <https://www.science.org/doi/10.1126/science.1226337>, doi:10.1126/science.1226337.
- 530    Beck, H.E., McVicar, T.R., Vergopolan, N., Berg, A., Lutsko, N.J., Dufour, A., Zeng, Z., Jiang, X., van Dijk, A.I.J.M., Miralles, D.G., 2023. High-resolution (1 km) Köppen-Geiger maps for 1901–2099 based on constrained CMIP6 projections. *Scientific Data* 10. URL: <http://dx.doi.org/10.1038/s41597-023-02549-6>, doi:10.1038/s41597-023-02549-6.
- 531    Beguería, S., Vicente-Serrano, S.M., 2023. SPEI: Calculation of the Standardized Precipitation-Evapotranspiration Index. URL: <https://CRAN.R-project.org/package=SPEI>.
- 532    Boisier, J.P., Alvarez-Garreton, C., Cordero, R.R., Damiani, A., Gallardo, L., Garreaud, R.D., Lambert, F., Ramallo, C., Rojas, M., Rondanelli, R., 2018. Anthropogenic drying in central-southern Chile evidenced by long-term observations and climate model simulations. *Elementa* 6, 74. URL: <https://www.elementascience.org/article/10.1525/elementa.328/>, doi:10.1525/elementa.328.

- 551 Calvin, K., Dasgupta, D., Krinner, G., Mukherji, A., Thorne, P.W., Trisos, C., Romero, J., Aldunce, P., Barrett, K., Blanco,  
 552 G., Cheung, W.W., Connors, S., Denton, F., Diougue-Niang, A., Dodman, D., Garschagen, M., Geden, O., Hayward, B.,  
 553 Jones, C., Jotzo, F., Krug, T., Lasco, R., Lee, Y.Y., Masson-Delmotte, V., Meinshausen, M., Mintenbeck, K., Mokssit, A.,  
 554 Otto, F.E., Pathak, M., Pirani, A., Poloczanska, E., Pörtner, H.O., Revi, A., Roberts, D.C., Roy, J., Ruane, A.C., Skea,  
 555 J., Shukla, P.R., Slade, R., Slangen, A., Sokona, Y., Sörensson, A.A., Tignor, M., Van Vuuren, D., Wei, Y.M., Winkler,  
 556 H., Zhai, P., Zommers, Z., Hourcade, J.C., Johnson, F.X., Pachauri, S., Simpson, N.P., Singh, C., Thomas, A., Totin, E.,  
 557 Arias, P., Bustamante, M., Elgizouli, I., Flato, G., Howden, M., Méndez-Vallejo, C., Pereira, J.J., Pichs-Madruga, R., Rose,  
 558 S.K., Saheb, Y., Sánchez Rodríguez, R., Ürge Vorsatz, D., Xiao, C., Yassa, N., Alegría, A., Armour, K., Bednar-Friedl, B.,  
 559 Blok, K., Cissé, G., Dentener, F., Eriksen, S., Fischer, E., Garner, G., Guiavarch, C., Haasnot, M., Hansen, G., Hauser, M.,  
 560 Hawkins, E., Hermans, T., Kopp, R., Leprince-Ringuet, N., Lewis, J., Ley, D., Ludden, C., Niamir, L., Nicholls, Z., Some,  
 561 S., Szopa, S., Trewin, B., Van Der Wijst, K.I., Winter, G., Witting, M., Birt, A., Ha, M., Romero, J., Kim, J., Haites, E.F.,  
 562 Jung, Y., Stavins, R., Birt, A., Ha, M., Orendain, D.J.A., Ignon, L., Park, S., Park, Y., Reisinger, A., Cammaramo, D.,  
 563 Fischlin, A., Fuglestvedt, J.S., Hansen, G., Ludden, C., Masson-Delmotte, V., Matthews, J.R., Mintenbeck, K., Pirani, A.,  
 564 Poloczanska, E., Leprince-Ringuet, N., Péan, C., 2023. IPCC, 2023: Climate Change 2023: Synthesis Report. Contribution  
 565 of Working Groups I, II and III to the Sixth Assessment Report of the Intergovernmental Panel on Climate Change [Core  
 566 Writing Team, H. Lee and J. Romero (eds.)]. IPCC, Geneva, Switzerland. Technical Report. Intergovernmental Panel on  
 567 Climate Change (IPCC). URL: <https://www.ipcc.ch/report/ar6/syr/>.
- 568 Camps-Valls, G., Campos-Taberner, M., Moreno-Martinez, , Walther, S., Duveiller, G., Cescatti, A., Mahecha, M.D., Muñoz-  
 569 Marí, J., García-Haro, F.J., Guanter, L., Jung, M., Gamon, J.A., Reichstein, M., Running, S.W., 2021. A unified vegetation  
 570 index for quantifying the terrestrial biosphere. *Science Advances* 7, eabc7447. URL: <https://www.science.org/doi/10.1126/sciadv.abc7447>, doi:[10.1126/sciadv.abc7447](https://doi.org/10.1126/sciadv.abc7447).
- 571 Chamling, M., Bera, B., 2020. Spatio-temporal Patterns of Land Use/Land Cover Change in the Bhutan–Bengal Foothill Region  
 572 Between 1987 and 2019: Study Towards Geospatial Applications and Policy Making. *Earth Systems and Environment* 4,  
 573 117–130. URL: <http://link.springer.com/10.1007/s41748-020-00150-0>, doi:[10.1007/s41748-020-00150-0](https://doi.org/10.1007/s41748-020-00150-0).
- 574 Chatterjee, S., Desai, A.R., Zhu, J., Townsend, P.A., Huang, J., 2022. Soil moisture as an essential component for delineating  
 575 and forecasting agricultural rather than meteorological drought. *Remote Sensing of Environment* 269, 112833. URL:  
 576 <https://linkinghub.elsevier.com/retrieve/pii/S0034425721005538>, doi:[10.1016/j.rse.2021.112833](https://doi.org/10.1016/j.rse.2021.112833).
- 577 Chen, J., Shao, Z., Huang, X., Zhuang, Q., Dang, C., Cai, B., Zheng, X., Ding, Q., 2022. Assessing the impact of drought-  
 578 land cover change on global vegetation greenness and productivity. *Science of The Total Environment* 852, 158499. URL:  
 579 <https://linkinghub.elsevier.com/retrieve/pii/S004896972205598X>, doi:[10.1016/j.scitotenv.2022.158499](https://doi.org/10.1016/j.scitotenv.2022.158499).
- 580 Crausbay, S.D., Ramirez, A.R., Carter, S.L., Cross, M.S., Hall, K.R., Bathke, D.J., Betancourt, J.L., Colt, S., Cravens, A.E.,  
 581 Dalton, M.S., Dunham, J.B., Hay, L.E., Hayes, M.J., McEvoy, J., McNutt, C.A., Moritz, M.A., Nislow, K.H., Raheem, N.,  
 582 Sanford, T., 2017. Defining Ecological Drought for the Twenty-First Century. *Bulletin of the American Meteorological Society*  
 583 98, 2543–2550. URL: <https://journals.ametsoc.org/view/journals/bams/98/12/bams-d-16-0292.1.xml>, doi:[10.1175/BAMS-D-16-0292.1](https://doi.org/10.1175/BAMS-D-16-0292.1). publisher: American Meteorological Society.
- 584 Dai, M., Huang, S., Huang, Q., Leng, G., Guo, Y., Wang, L., Fang, W., Li, P., Zheng, X., 2020. Assessing agricultural drought  
 585 risk and its dynamic evolution characteristics. *Agricultural Water Management* 231, 106003. URL: <https://linkinghub.elsevier.com/retrieve/pii/S0378377419316531>, doi:[10.1016/j.agwat.2020.106003](https://doi.org/10.1016/j.agwat.2020.106003).
- 586 Didan, K., 2015. MOD13Q1 MODIS/Terra Vegetation Indices 16-Day L3 Global 250m SIN Grid V006. Technical Report.  
 587 NASA EOSDIS Land Processes DAAC. doi:<http://dx.doi.org/10.5067/MODIS/MOD13Q1.006>.
- 588 Farahmand, A., AghaKouchak, A., 2015. A generalized framework for deriving nonparametric standardized drought indicators.  
 589 *Advances in Water Resources* 76, 140–145. URL: <https://linkinghub.elsevier.com/retrieve/pii/S0309170814002322>, doi:[10.1016/j.advwatres.2014.11.012](https://doi.org/10.1016/j.advwatres.2014.11.012).
- 590 Fathi-Taperasht, A., Shafizadeh-Moghadam, H., Minaei, M., Xu, T., 2022. Influence of drought duration and severity on  
 591 drought recovery period for different land cover types: evaluation using MODIS-based indices. *Ecological Indicators* 141,  
 592 109146. URL: <https://linkinghub.elsevier.com/retrieve/pii/S1470160X22006185>, doi:[10.1016/j.ecolind.2022.109146](https://doi.org/10.1016/j.ecolind.2022.109146).
- 593 Ford, T.W., Otkin, J.A., Quiring, S.M., Lisonbee, J., Woloszyn, M., Wang, J., Zhong, Y., 2023. Flash Drought Indicator  
 594 Intercomparison in the United States. *Journal of Applied Meteorology and Climatology* 62, 1713–1730. URL: <https://journals.ametsoc.org/view/journals/apme/62/12/JAMC-D-23-0081.1.xml>, doi:[10.1175/JAMC-D-23-0081.1](https://doi.org/10.1175/JAMC-D-23-0081.1).
- 595 Fuentes, I., Fuster, R., Avilés, D., Vervoort, W., 2021. Water scarcity in central Chile: the effect of climate and land cover  
 596 changes on hydrologic resources. *Hydrological Sciences Journal* 66, 1028–1044. URL: <https://www.tandfonline.com/doi/full/10.1080/02626667.2021.1903475>, doi:[10.1080/02626667.2021.1903475](https://doi.org/10.1080/02626667.2021.1903475).
- 597 Garreaud, R., Alvarez-Garreton, C., Barichivich, J., Boisier, J.P., Christie, D., Galleguillos, M., LeQuesne, C., McPhee,  
 598 J., Zambrano-Bigiarini, M., 2017. The 2010–2015 mega drought in Central Chile: Impacts on regional hydroclimate and  
 599 vegetation. *Hydrology and Earth System Sciences Discussions* 2017, 1–37. URL: <http://www.hydrol-earth-syst-sci-discuss.net/hess-2017-191/>, doi:[10.5194/hess-2017-191](https://doi.org/10.5194/hess-2017-191).
- 600 Garreaud, R.D., 2009. The Andes climate and weather. *Advances in Geosciences* 22, 3–11. URL: <https://adgeo.copernicus.org/articles/22/3/2009/>, doi:[10.5194/adgeo-22-3-2009](https://doi.org/10.5194/adgeo-22-3-2009).
- 601 Gebrechorkos, S.H., Peng, J., Dyer, E., Miralles, D.G., Vicente-Serrano, S.M., Funk, C., Beck, H.E., Asfaw, D.T., Singer, M.B.,  
 602 Dadson, S.J., 2023. Global high-resolution drought indices for 1981–2022. *Earth System Science Data* 15, 5449–5466. URL:  
 603 <https://essd.copernicus.org/articles/15/5449/2023/>, doi:[10.5194/essd-15-5449-2023](https://doi.org/10.5194/essd-15-5449-2023).
- 604 Hao, Z., AghaKouchak, A., 2013. Multivariate Standardized Drought Index: A parametric multi-index model. *Advances in Water  
 605 Resources* 57, 12–18. URL: <https://linkinghub.elsevier.com/retrieve/pii/S0309170813000493>, doi:[10.1016/j.advwatres.2013.03.009](https://doi.org/10.1016/j.advwatres.2013.03.009).
- 606 Hargreaves, G.H., 1994. Defining and Using Reference Evapotranspiration. *Journal of Irrigation and Drainage Engineering* 120,

- 616 1132–1139. URL: <https://ascelibrary.org/doi/10.1061/%28ASCE%290733-9437%281994%29120%3A6%281132%29>, doi:10.1061/(ASCE)0733-9437(1994)120:6(1132).
- 617 Hargreaves, G.H., Samani, Z.A., 1985. Reference crop evapotranspiration from temperature. Applied engineering in agriculture 1, 96–99.
- 618 Heim, R.R., 2002. A Review of Twentieth-Century Drought Indices Used in the United States. Bulletin of the American Meteorological Society 83, 1149–1166. URL: <https://journals.ametsoc.org/doi/10.1175/1520-0477-83.8.1149>, doi:10.1175/1520-0477-83.8.1149.
- 619 Helman, D., Mussery, A., Lensky, I.M., Leu, S., 2014. Detecting changes in biomass productivity in a different land management regimes in drylands using satellite-derived vegetation index. Soil Use and Management 30, 32–39. URL: <https://bsssjournals.onlinelibrary.wiley.com/doi/10.1111/sum.12099>, doi:10.1111/sum.12099.
- 620 Hijmans, R.J., 2023. terra: Spatial Data Analysis. URL: <https://CRAN.R-project.org/package=terra>.
- 621 Hobbins, M.T., Wood, A., McEvoy, D.J., Huntington, J.L., Morton, C., Anderson, M., Hain, C., 2016. The Evaporative Demand Drought Index. Part I: Linking Drought Evolution to Variations in Evaporative Demand. Journal of Hydrometeorology 17, 1745–1761. URL: <http://journals.ametsoc.org/doi/10.1175/JHM-D-15-0121.1>, doi:10.1175/JHM-D-15-0121.1.
- 622 Homer, C., Dewitz, J., Jin, S., Xian, G., Costello, C., Danielson, P., Gass, L., Funk, M., Wickham, J., Stelman, S., Auch, R., Riitters, K., 2020. Conterminous United States land cover change patterns 2001–2016 from the 2016 National Land Cover Database. ISPRS Journal of Photogrammetry and Remote Sensing 162, 184–199. URL: <https://linkinghub.elsevier.com/retrieve/pii/S0924271620300587>, doi:10.1016/j.isprsjprs.2020.02.019.
- 623 Hufkens, K., Stauffer, R., Campitelli, E., 2019. The ecmwfr package: an interface to ECMWF API endpoints. URL: <https://bluegreen-labs.github.io/ecmwfr/>.
- 624 Humphrey, V., Berg, A., Ciais, P., Gentine, P., Jung, M., Reichstein, M., Seneviratne, S.I., Frankenberg, C., 2021. Soil moisture–atmosphere feedback dominates land carbon uptake variability. Nature 592, 65–69. URL: <https://www.nature.com/articles/s41586-021-03325-5>, doi:10.1038/s41586-021-03325-5.
- 625 IPCC, 2013. Climate Change 2013: The Physical Science Basis. Contribution of Working Group I to the Fifth Assessment Report of the Intergovernmental Panel on Climate Change. Cambridge University Press, Cambridge, UK; New York, USA. URL: [www.climatechange2013.org](http://www.climatechange2013.org), doi:10.1017/CBO9781107415324.
- 626 Jiang, W., Wang, L., Feng, L., Zhang, M., Yao, R., 2020. Drought characteristics and its impact on changes in surface vegetation from 1981 to 2015 in the Yangtze River Basin, China. International Journal of Climatology 40, 3380–3397. URL: <https://rmets.onlinelibrary.wiley.com/doi/10.1002/joc.6403>, doi:10.1002/joc.6403.
- 627 Kendall, M., 1975. Rank correlation methods (4th ed. 2d impression). Griffin.
- 628 Kogan, F., Guo, W., Yang, W., 2020. Near 40-year drought trend during 1981–2019 earth warming and food security. Geomatics, Natural Hazards and Risk 11, 469–490. URL: <https://www.tandfonline.com/doi/full/10.1080/19475705.2020.1730452>, doi:10.1080/19475705.2020.1730452.
- 629 Kuhn, M., Wickham, H., 2020. Tidymodels: a collection of packages for modeling and machine learning using tidyverse principles. URL: <https://www.tidymodels.org>.
- 630 Laimighofer, J., Laaha, G., 2022. How standard are standardized drought indices? Uncertainty components for the SPI & SPEI case. Journal of Hydrology 613, 128385. URL: <https://linkinghub.elsevier.com/retrieve/pii/S0022169422009544>, doi:10.1016/j.jhydrol.2022.128385.
- 631 Li, H., Choy, S., Zaminpardaz, S., Wang, X., Liang, H., Zhang, K., 2024. Flash drought monitoring using diurnal-provided evaporative demand drought index. Journal of Hydrology 633, 130961. URL: <https://linkinghub.elsevier.com/retrieve/pii/S002216942400355X>, doi:10.1016/j.jhydrol.2024.130961.
- 632 Li, W., Migliavacca, M., Forkel, M., Denissen, J.M.C., Reichstein, M., Yang, H., Duveiller, G., Weber, U., Orth, R., 2022. Widespread increasing vegetation sensitivity to soil moisture. Nature Communications 13, 3959. URL: <https://www.nature.com/articles/s41467-022-31667-9>, doi:10.1038/s41467-022-31667-9.
- 633 Liu, X., Yu, S., Yang, Z., Dong, J., Peng, J., 2024. The first global multi-timescale daily SPEI dataset from 1982 to 2021. Scientific Data 11, 223. URL: <https://www.nature.com/articles/s41597-024-03047-z>, doi:10.1038/s41597-024-03047-z.
- 634 Luebert, F., Pliscott, P., 2022. The vegetation of Chile and the EcoVeg approach in the context of the International Vegetation Classification project. Vegetation Classification and Survey 3, 15–28. URL: <https://vcs.pensoft.net/article/67893/>, doi:10.3897/VCS.67893.
- 635 Luo, L., Apps, D., Arcand, S., Xu, H., Pan, M., Hoerling, M., 2017. Contribution of temperature and precipitation anomalies to the California drought during 2012–2015. Geophysical Research Letters 44, 3184–3192. URL: <https://agupubs.onlinelibrary.wiley.com/doi/10.1002/2016GL072027>, doi:10.1002/2016GL072027.
- 636 Luyssaert, S., Jammet, M., Stoy, P.C., Estel, S., Pongratz, J., Ceschia, E., Churkina, G., Don, A., Erb, K., Ferlicoq, M., Gielen, B., Grünwald, T., Houghton, R.A., Klumpp, K., Knohl, A., Kolb, T., Kuemmerle, T., Laurila, T., Lohila, A., Loustau, D., McGrath, M.J., Meyfroidt, P., Moors, E.J., Naudts, K., Novick, K., Otto, J., Pilegaard, K., Pio, C.A., Rambal, S., Rebmann, C., Ryder, J., Suyker, A.E., Varlagin, A., Wattenbach, M., Dolman, A.J., 2014. Land management and land-cover change have impacts of similar magnitude on surface temperature. Nature Climate Change 4, 389–393. URL: <https://www.nature.com/articles/nclimate2196>, doi:10.1038/nclimate2196.
- 637 Masson-Delmotte, V., P.Z.A.P.S.L.C.C.P.S.B.N.C.Y.C.L.G.M.I.G.M.H.K.L.E.L.J.B.R.M.T.K.M.T.W.O.Y.R.Y.a.B.Z.e., 2021. IPCC, 2021: Climate Change 2021: The Physical Science Basis. Contribution of Working Group I to the Sixth Assessment Report of the Intergovernmental Panel on Climate Change. Technical Report. URL: <https://www.ipcc.ch/>. publication Title: Cambridge University Press. In Press.
- 638 McEvoy, D.J., Huntington, J.L., Hobbins, M.T., Wood, A., Morton, C., Anderson, M., Hain, C., 2016. The Evaporative Demand Drought Index. Part II: CONUS-Wide Assessment against Common Drought Indicators. Journal of Hydrometeorology 17, 1763–1779. URL: <http://journals.ametsoc.org/doi/10.1175/JHM-D-15-0122.1>, doi:10.1175/JHM-D-15-0122.1.

- 681 Meroni, M., Rembold, F., Fasbender, D., Vrieling, A., 2017. Evaluation of the Standardized Precipitation Index as an early  
 682 predictor of seasonal vegetation production anomalies in the Sahel. *Remote Sensing Letters* 8, 301–310. URL: <http://www.tandfonline.com/doi/abs/10.1080/2150704X.2016.1264020>, doi:[10.1080/2150704X.2016.1264020](https://doi.org/10.1080/2150704X.2016.1264020).
- 683 Miranda, A., Lara, A., Altamirano, A., Di Bella, C., González, M.E., Julio Camarero, J., 2020. Forest browning trends in  
 684 response to drought in a highly threatened mediterranean landscape of South America. *Ecological Indicators* 115, 106401.  
 685 URL: <https://linkinghub.elsevier.com/retrieve/pii/S1470160X20303381>, doi:[10.1016/j.ecolind.2020.106401](https://doi.org/10.1016/j.ecolind.2020.106401).
- 686 Muñoz-Sabater, J., Dutra, E., Agustí-Panareda, A., Albergel, C., Arduini, G., Balsamo, G., Boussetta, S., Choulga, M.,  
 687 Harrigan, S., Hersbach, H., Martens, B., Miralles, D.G., Piles, M., Rodríguez-Fernández, N.J., Zsoter, E., Buontempo, C.,  
 688 Thépaut, J.N., 2021. ERA5-Land: a state-of-the-art global reanalysis dataset for land applications. *Earth System Science  
 689 Data* 13, 4349–4383. URL: <https://essd.copernicus.org/articles/13/4349/2021/>, doi:[10.5194/essd-13-4349-2021](https://doi.org/10.5194/essd-13-4349-2021).
- 690 Narasimhan, B., Srinivasan, R., 2005. Development and evaluation of Soil Moisture Deficit Index (SMDI) and Evapotranspiration  
 691 Deficit Index (ETDI) for agricultural drought monitoring. *Agricultural and Forest Meteorology* 133, 69–88. URL:  
 692 <https://linkinghub.elsevier.com/retrieve/pii/S0168192305001565>, doi:[10.1016/j.agrformet.2005.07.012](https://doi.org/10.1016/j.agrformet.2005.07.012).
- 693 Nicolai-Shaw, N., Zscheischler, J., Hirsch, M., Gudmundsson, L., Seneviratne, S.I., 2017. A drought event composite analysis  
 694 using satellite remote-sensing based soil moisture. *Remote Sensing of Environment* 203, 216–225. URL: <https://linkinghub.elsevier.com/retrieve/pii/S0034425717302729>, doi:[10.1016/j.rse.2017.06.014](https://doi.org/10.1016/j.rse.2017.06.014).
- 695 Noguera, I., Vicente-Serrano, S.M., Domínguez-Castro, F., 2022. The Rise of Atmospheric Evaporative Demand Is Increasing  
 696 Flash Droughts in Spain During the Warm Season. *Geophysical Research Letters* 49, e2021GL097703. URL: <https://agupubs.onlinelibrary.wiley.com/doi/10.1029/2021GL097703>, doi:[10.1029/2021GL097703](https://doi.org/10.1029/2021GL097703).
- 697 Paruelo, J.M., Texeira, M., Staiano, L., Mastrángelo, M., Amdan, L., Gallego, F., 2016. An integrative index of Ecosystem  
 698 Services provision based on remotely sensed data. *Ecological Indicators* 71, 145–154. URL: <https://www.sciencedirect.com/science/article/pii/S1470160X16303843>, doi:[10.1016/J.ECOLIND.2016.06.054](https://doi.org/10.1016/J.ECOLIND.2016.06.054). publisher: Elsevier.
- 699 Pebesma, E., 2018. Simple Features for R: Standardized Support for Spatial Vector Data. *The R Journal* 10, 439–446. URL:  
 700 <https://doi.org/10.32614/RJ-2018-009>, doi:[10.32614/RJ-2018-009](https://doi.org/10.32614/RJ-2018-009).
- 701 Pebesma, E., Bivand, R., 2023. Spatial Data Science: With applications in R. Chapman and Hall/CRC, London. URL:  
 702 <https://r-spatial.org/book/>.
- 703 Peng, D., Zhang, B., Wu, C., Huete, A.R., Gonsamo, A., Lei, L., Ponce-Campos, G.E., Liu, X., Wu, Y., 2017. Country-level  
 704 net primary production distribution and response to drought and land cover change. *Science of The Total Environment* 574,  
 705 65–77. URL: <https://linkinghub.elsevier.com/retrieve/pii/S0048969716319507>, doi:[10.1016/j.scitotenv.2016.09.033](https://doi.org/10.1016/j.scitotenv.2016.09.033).
- 706 Pitman, A.J., De Noblet-Ducoudré, N., Avila, F.B., Alexander, L.V., Boisier, J.P., Brovkin, V., Delire, C., Cruz, F., Donat,  
 707 M.G., Gayler, V., Van Den Hurk, B., Reick, C., Voldoire, A., 2012. Effects of land cover change on temperature and  
 708 rainfall extremes in multi-model ensemble simulations. *Earth System Dynamics* 3, 213–231. URL: <https://esd.copernicus.org/articles/3/213/2012/>, doi:[10.5194/esd-3-213-2012](https://doi.org/10.5194/esd-3-213-2012).
- 709 Potopová, V., Stepánek, P., Mozný, M., Türkott, L., Soukup, J., 2015. Performance of the standarised precipitation evapotranspiration  
 710 index at various lags for agricultural drought risk assessment in the {C}zech {R}epublic. *Agricultural and Forest  
 711 Meteorology* 202, 26–38.
- 712 R Core Team, 2023. R: A Language and Environment for Statistical Computing. R Foundation for Statistical Computing,  
 713 Vienna, Austria. URL: <https://www.R-project.org/>.
- 714 Rhee, J., Im, J., Carbone, G.J., 2010. Monitoring agricultural drought for arid and humid regions using multi-sensor remote  
 715 sensing data. *Remote Sensing of Environment* 114, 2875–2887. URL: <http://www.sciencedirect.com/science/article/pii/S003442571000221X>, doi:[10.1016/j.rse.2010.07.005](https://doi.org/10.1016/j.rse.2010.07.005).
- 716 Samaniego, L., Thober, S., Kumar, R., Wanders, N., Rakovec, O., Pan, M., Zink, M., Sheffield, J., Wood, E.F., Marx, A.,  
 717 2018. Anthropogenic warming exacerbates European soil moisture droughts. *Nature Climate Change* 8, 421–426. URL:  
 718 <https://www.nature.com/articles/s41558-018-0138-5>, doi:[10.1038/s41558-018-0138-5](https://doi.org/10.1038/s41558-018-0138-5).
- 719 Sen, P.K., 1968. Estimates of the Regression Coefficient Based on Kendall's Tau. *Journal of the American Statistical Association*  
 720 63, 1379–1389. URL: <http://www.tandfonline.com/doi/abs/10.1080/01621459.1968.10480934>, doi:[10.1080/01621459.1968.10480934](https://doi.org/10.1080/01621459.1968.10480934).
- 721 Senf, C., Buras, A., Zang, C.S., Rammig, A., Seidl, R., 2020. Excess forest mortality is consistently linked to drought  
 722 across Europe. *Nature Communications* 11, 6200. URL: <https://www.nature.com/articles/s41467-020-19924-1>, doi:[10.1038/s41467-020-19924-1](https://doi.org/10.1038/s41467-020-19924-1).
- 723 Slette, I.J., Post, A.K., Awad, M., Even, T., Punzalan, A., Williams, S., Smith, M.D., Knapp, A.K., 2019. How ecologists  
 724 define drought, and why we should do better. *Global Change Biology* 25, 3193–3200. URL: <https://onlinelibrary.wiley.com/doi/10.1111/gcb.14747>, doi:[10.1111/gcb.14747](https://doi.org/10.1111/gcb.14747).
- 725 Song, X.P., Hansen, M.C., Stehman, S.V., Potapov, P.V., Tyukavina, A., Vermote, E.F., Townshend, J.R., 2018. Global land  
 726 change from 1982 to 2016. *Nature* 560, 639–643. URL: <https://www.nature.com/articles/s41586-018-0411-9>, doi:[10.1038/s41586-018-0411-9](https://doi.org/10.1038/s41586-018-0411-9).
- 727 Souza, A.G.S.S., Ribeiro Neto, A., Souza, L.L.D., 2021. Soil moisture-based index for agricultural drought assessment: SMADI  
 728 application in Pernambuco State-Brazil. *Remote Sensing of Environment* 252, 112124. URL: <https://linkinghub.elsevier.com/retrieve/pii/S0034425720304971>, doi:[10.1016/j.rse.2020.112124](https://doi.org/10.1016/j.rse.2020.112124).
- 729 Taucare, M., Viguier, B., Figueiroa, R., Daniele, L., 2024. The alarming state of Central Chile's groundwater resources: A  
 730 paradigmatic case of a lasting overexploitation. *Science of The Total Environment* 906, 167723. URL: <https://linkinghub.elsevier.com/retrieve/pii/S0048969723063507>, doi:[10.1016/j.scitotenv.2023.167723](https://doi.org/10.1016/j.scitotenv.2023.167723).
- 731 Tennekes, M., 2018. tmap: Thematic Maps in R. *Journal of Statistical Software* 84, 1–39. doi:[10.18637/jss.v084.i06](https://doi.org/10.18637/jss.v084.i06).
- 732 Urrutia-Jalabert, R., González, M.E., González-Reyes, A., Lara, A., Garreaud, R., 2018. Climate variability and forest fires in  
 733 central and south-central Chile. *Ecosphere* 9, e02171. URL: <https://esajournals.onlinelibrary.wiley.com/doi/10.1002/ecs2.02171>.

- 746                  2171, doi:[10.1002/ecs2.2171](https://doi.org/10.1002/ecs2.2171).
- 747 Van Loon, A.F., Gleeson, T., Clark, J., Van Dijk, A.I., Stahl, K., Hannaford, J., Di Baldassarre, G., Teuling, A.J., Tallaksen,  
748 L.M., Uijlenhoet, R., Hannah, D.M., Sheffield, J., Svoboda, M., Verbeiren, B., Wagener, T., Rangecroft, S., Wanders, N.,  
749 Van Lanen, H.A., 2016. Drought in the Anthropocene. *Nature Geoscience* 9, 89–91. doi:[10.1038/ngeo2646](https://doi.org/10.1038/ngeo2646).
- 750 Van Loon, A.F., Van Huijgevoort, M.H.J., Van Lanen, H.A.J., 2012. Evaluation of drought propagation in an ensemble mean  
751 of large-scale hydrological models. *Hydrology and Earth System Sciences* 16, 4057–4078. URL: <https://hess.copernicus.org/articles/16/4057/2012/>, doi:[10.5194/hess-16-4057-2012](https://doi.org/10.5194/hess-16-4057-2012).
- 753 Venegas-González, A., Juñent, F.R., Gutiérrez, A.G., Filho, M.T., 2018. Recent radial growth decline in response to increased  
754 drought conditions in the northernmost Nothofagus populations from South America. *Forest Ecology and Management* 409,  
755 94–104. URL: <https://linkinghub.elsevier.com/retrieve/pii/S0378112717313993>, doi:[10.1016/j.foreco.2017.11.006](https://doi.org/10.1016/j.foreco.2017.11.006).
- 756 Venegas-González, A., Muñoz, A.A., Carpintero-Gibson, S., González-Reyes, A., Schneider, I., Gipolou-Zuñiga, T., Aguilera-  
757 Betti, I., Roig, F.A., 2023. Sclerophyllous Forest Tree Growth Under the Influence of a Historic Megadrought in the  
758 Mediterranean Ecoregion of Chile. *Ecosystems* 26, 344–361. URL: <https://link.springer.com/10.1007/s10021-022-00760-x>,  
759 doi:[10.1007/s10021-022-00760-x](https://doi.org/10.1007/s10021-022-00760-x).
- 760 Vicente-Serrano, S.M., Azorin-Molina, C., Sanchez-Lorenzo, A., Revuelto, J., López-Moreno, J.I., González-Hidalgo, J.C.,  
761 Moran-Tejeda, E., Espejo, F., 2014. Reference evapotranspiration variability and trends in Spain, 1961–2011. *Global  
762 and Planetary Change* 121, 26–40. URL: <https://linkinghub.elsevier.com/retrieve/pii/S0921818114001180>, doi:[10.1016/j.gloplacha.2014.06.005](https://doi.org/10.1016/j.gloplacha.2014.06.005).
- 764 Vicente-Serrano, S.M., Beguería, S., López-Moreno, J.I., 2010. A multiscalar drought index sensitive to global warming: The  
765 standardized precipitation evapotranspiration index. *Journal of Climate* 23, 1696–1718. URL: <http://dx.doi.org/10.1175/2009JCLI2909.1>, doi:[10.1175/2009JCLI2909.1](https://doi.org/10.1175/2009JCLI2909.1).
- 767 Vicente-Serrano, S.M., Peña-Angulo, D., Beguería, S., Domínguez-Castro, F., Tomás-Burguera, M., Noguera, I., Gimeno-  
768 Sotelo, L., El Kenawy, A., 2022. Global drought trends and future projections. *Philosophical Transactions of the Royal  
769 Society A: Mathematical, Physical and Engineering Sciences* 380, 20210285. URL: <https://royalsocietypublishing.org/doi/10.1098/rsta.2021.0285>, doi:[10.1098/rsta.2021.0285](https://doi.org/10.1098/rsta.2021.0285).
- 771 Vicente-Serrano, S.M., McVicar, T.R., Miralles, D.G., Yang, Y., Tomas-Burguera, M., 2020. Unraveling the influence of  
772 atmospheric evaporative demand on drought and its response to climate change. *WIREs Climate Change* 11, e632. URL:  
773 <https://wires.onlinelibrary.wiley.com/doi/10.1002/wcc.632>, doi:[10.1002/wcc.632](https://doi.org/10.1002/wcc.632).
- 774 Wickham, H., Averick, M., Bryan, J., Chang, W., McGowan, L.D., François, R., Gromelund, G., Hayes, A., Henry, L., Hester,  
775 J., Kuhn, M., Pedersen, T.L., Miller, E., Bache, S.M., Müller, K., Ooms, J., Robinson, D., Seidel, D.P., Spinu, V., Takahashi,  
776 K., Vaughan, D., Wilke, C., Woo, K., Yutani, H., 2019. Welcome to the tidyverse. *Journal of Open Source Software* 4, 1686.  
777 doi:[10.21105/joss.01686](https://doi.org/10.21105/joss.01686).
- 778 Wilhite, D.A., Glantz, M.H., 1985. Understanding: The drought phenomenon: The role of definitions. *Water International* 10,  
779 111–120. URL: <http://dx.doi.org/10.1080/02508068508686328>, doi:[10.1080/02508068508686328](https://doi.org/10.1080/02508068508686328).
- 780 Wilks, D.S., 2011. Empirical distributions and exploratory data analysis. *Statistical Methods in the Atmospheric Sciences* 100.
- 781 Winkler, K., Fuchs, R., Rounsevell, M., Herold, M., 2021. Global land use changes are four times greater than previously  
782 estimated. *Nature Communications* 12, 2501. URL: <https://www.nature.com/articles/s41467-021-22702-2>, doi:[10.1038/s41467-021-22702-2](https://doi.org/10.1038/s41467-021-22702-2).
- 784 WMO, Svoboda, M., Hayes, M., Wood, D.A., 2012. Standardized Precipitation Index User Guide. WMO, Geneva. URL:  
785 [http://library.wmo.int/opac/index.php?lvl=notice\\_display&id=13682](http://library.wmo.int/opac/index.php?lvl=notice_display&id=13682). series Title: WMO Publication Title: WMO-No.  
786 1090 © Issue: 1090.
- 787 Wright, M.N., Ziegler, A., 2017. ranger: A Fast Implementation of Random Forests for High Dimensional Data in C++ and  
788 R. *Journal of Statistical Software* 77, 1–17. doi:[10.18637/jss.v077.i01](https://doi.org/10.18637/jss.v077.i01).
- 789 Wu, C., Zhong, L., Yeh, P.J.F., Gong, Z., Lv, W., Chen, B., Zhou, J., Li, J., Wang, S., 2024. An evaluation framework  
790 for quantifying vegetation loss and recovery in response to meteorological drought based on SPEI and NDVI. *Science of  
791 The Total Environment* 906, 167632. URL: <https://linkinghub.elsevier.com/retrieve/pii/S0048969723062599>, doi:[10.1016/j.scitotenv.2023.167632](https://doi.org/10.1016/j.scitotenv.2023.167632).
- 793 Xiao, C., Zaehle, S., Yang, H., Wigneron, J.P., Schmullius, C., Bastos, A., 2023. Land cover and management effects on  
794 ecosystem resistance to drought stress. *Earth System Dynamics* 14, 1211–1237. URL: <https://esd.copernicus.org/articles/14/1211/2023/>, doi:[10.5194/esd-14-1211-2023](https://doi.org/10.5194/esd-14-1211-2023).
- 796 Yang, J., Huang, X., 2021. The 30 m annual land cover dataset and its dynamics in China from 1990 to 2019. *Earth System  
797 Science Data* 13, 3907–3925. URL: <https://essd.copernicus.org/articles/13/3907/2021/>, doi:[10.5194/essd-13-3907-2021](https://doi.org/10.5194/essd-13-3907-2021).
- 798 Zambrano, F., 2023. Four decades of satellite data for agricultural drought monitoring throughout the growing season in Central  
799 Chile, in: Vijay P. Singh Deepak Jhajharia, R.M., Kumar, R. (Eds.), *Integrated Drought Management*, Two Volume Set.  
800 CRC Press, p. 28.
- 801 Zambrano, F., Lillo-Saavedra, M., Verbist, K., Lagos, O., 2016. Sixteen years of agricultural drought assessment of the  
802 biobío region in chile using a 250 m resolution vegetation condition index (VCI). *Remote Sensing* 8, 1–20. URL: <http://www.mdpi.com/2072-4292/8/6/530>, doi:[10.3390/rs8060530](https://doi.org/10.3390/rs8060530). publisher: Multidisciplinary Digital Publishing Institute.
- 804 Zambrano, F., Vrieling, A., Nelson, A., Meroni, M., Tadesse, T., 2018. Prediction of drought-induced reduction of agricultural  
805 productivity in Chile from MODIS, rainfall estimates, and climate oscillation indices. *Remote Sensing of Environment*  
806 219, 15–30. URL: <https://www.sciencedirect.com/science/article/pii/S0034425718304541>, doi:[10.1016/j.rse.2018.10.006](https://doi.org/10.1016/j.rse.2018.10.006).  
807 publisher: Elsevier.
- 808 Zhang, W., Wei, F., Horion, S., Fensholt, R., Forkel, M., Brandt, M., 2022. Global quantification of the bidirectional de-  
809 pendency between soil moisture and vegetation productivity. *Agricultural and Forest Meteorology* 313, 108735. URL:  
810 <https://linkinghub.elsevier.com/retrieve/pii/S0168192321004214>, doi:[10.1016/j.agrformet.2021.108735](https://doi.org/10.1016/j.agrformet.2021.108735).

- 811 Zhao, Y., Feng, D., Yu, L., Wang, X., Chen, Y., Bai, Y., Hernández, H.J., Galleguillos, M., Estades, C., Biging, G.S., Radke,  
812 J.D., Gong, P., 2016. Detailed dynamic land cover mapping of Chile: Accuracy improvement by integrating multi-temporal  
813 data. *Remote Sensing of Environment* 183, 170–185. URL: <https://linkinghub.elsevier.com/retrieve/pii/S0034425716302188>,  
814 doi:[10.1016/j.rse.2016.05.016](https://doi.org/10.1016/j.rse.2016.05.016).
- 815 Zhou, K., Li, J., Zhang, T., Kang, A., 2021. The use of combined soil moisture data to characterize agricultural drought  
816 conditions and the relationship among different drought types in China. *Agricultural Water Management* 243, 106479. URL:  
817 <https://linkinghub.elsevier.com/retrieve/pii/S0378377420305965>, doi:[10.1016/j.agwat.2020.106479](https://doi.org/10.1016/j.agwat.2020.106479).